



HAL
open science

Geophysical and geochemical analysis of shallow gas and an associated pockmark field in Bantry Bay, Co. Cork, Ireland

Sean Jordan, Shane O'Reilly, Daniel Praeg, Dayton Dove, Lorenzo Facchin, Roberto Romeo, Michal Szpak, Xavier Monteys, B.T. Murphy, Gill Scott, et al.

► To cite this version:

Sean Jordan, Shane O'Reilly, Daniel Praeg, Dayton Dove, Lorenzo Facchin, et al.. Geophysical and geochemical analysis of shallow gas and an associated pockmark field in Bantry Bay, Co. Cork, Ireland. *Estuarine, Coastal and Shelf Science*, 2019, 225, pp.106232. 10.1016/j.ecss.2019.05.014 . hal-02272568

HAL Id: hal-02272568

<https://hal.science/hal-02272568>

Submitted on 29 Aug 2019

HAL is a multi-disciplinary open access archive for the deposit and dissemination of scientific research documents, whether they are published or not. The documents may come from teaching and research institutions in France or abroad, or from public or private research centers.

L'archive ouverte pluridisciplinaire **HAL**, est destinée au dépôt et à la diffusion de documents scientifiques de niveau recherche, publiés ou non, émanant des établissements d'enseignement et de recherche français ou étrangers, des laboratoires publics ou privés.

Manuscript Details

Manuscript number ECSS_2019_96_R2

Title Geophysical and geochemical analysis of shallow gas and an associated pockmark field in Bantry Bay, Co. Cork, Ireland.

Article type Research Paper

Abstract

An integrated geophysical, geological, and geochemical investigation of seabed fluid venting was carried out in upper Bantry Bay, a large marine inlet on the southwest coast of Ireland. The results provide evidence of the seafloor venting of gas rich fluids, resulting in the formation of a pockmark field identified here for the first time. The pockmarks occur in an area where sub-bottom profiles provide evidence of chimney-like features interpreted to record upward gas migration through Quaternary sediments to the seafloor. Three vibrocores up to 6 m long were acquired in water depths of 24-34 m, two from the pockmark field and one from outside. Methane of predominantly biogenic origin was quantified in all three cores by headspace analysis of sediment sub-samples. Well-defined sulfate methane transition zones (SMTZs) were observed in two of the cores, the shallowest (1.25 m) inside the pockmark field and the other (3.75 m) outside. It is likely that an SMTZ occurs at the location of the third core, also within the pockmark field, although beneath the samples obtained during this study. Gas release possibly from a combination of various faulting mechanisms and shallow methanogenesis appears to drive diffuse pore fluid migration across wide areas, while focused flow through the pockmarks may be related to gas originating from the Owenberg River Fault and methanogenesis of pre-glacial lacustrine sediments preserved in a bedrock basin. Analysis of phospholipid fatty acids (PLFAs) and archaeal isoprenoid hydrocarbons was used to investigate the microbial ecology of these sediments. Anaerobic oxidation of methane (AOM) may play a role in controlling release of CH₄ to the water column and atmosphere in this shallow gas setting, potentially mediated by syntrophic sulfate reducing bacteria (SRB) and anaerobic methanotrophic archaea (ANME).

Keywords Geophysics; biogeochemical processes; pockmarks; fluid migration; anaerobic oxidation of methane (AOM); lipid biomarkers

Taxonomy Oceanography, Methane

Corresponding Author Brian Kelleher

Corresponding Author's Institution Dublin City University

Order of Authors Sean Jordan, Shane O' Reilly, Daniel Praeg, Dayton Dove, Lorenzo Facchin, Roberto romeo, Michal Szpak, xavier monteys, Brian Murphy, Gill Scott, Stephen McCarron, Brian Kelleher

Suggested reviewers Alan Judd, Joseph Kelley, Aggeliki Georgiopoulou, Crispin Little

Submission Files Included in this PDF

File Name [File Type]

coverletterKelleher.doc [Cover Letter]

Response to reviewers [Rev].docx [Response to Reviewers]

Highlights (2).docx [Highlights]

Manuscript.docx [Manuscript File]

Figure 4.pdf [Figure]

Figure Captions (3).docx [Figure]

Fig 1 [Rev] pdf.pdf [Figure]

Figure 1 [Rev] tif.tif [Figure]

Figure 2 [Rev] pdf.pdf [Figure]

Figure 2 [Rev] tif.tif [Figure]

Figure 3.pdf [Figure]

Supporting Information [Rev].docx [Supporting File]

To view all the submission files, including those not included in the PDF, click on the manuscript title on your EVISE Homepage, then click 'Download zip file'.

Research Data Related to this Submission

There are no linked research data sets for this submission. The following reason is given:
Data will be made available on request

Highlights

- Acoustic data provided evidence for widespread fluid migration in a shallow marine bay in Co. Cork, Ireland including shallow gas deposits near the seabed.
- Fluid migration has led to the formation of a previously undescribed pockmark field within the bay.
- Ground-truthing confirmed that the fluid was methane which is likely both thermogenic and biogenic in origin, possibly derived from an underlying fault and methanogenesis of pre-glacial lacustrine sediments.
- Geochemical evidence suggests that microbial anaerobic oxidation of methane (AOM) plays a key role in controlling the release of methane to the atmosphere from the bay.

1
2
3
4 1 Geophysical and geochemical analysis of shallow gas and an associated
5
6 2 pockmark field in Bantry Bay, Co. Cork, Ireland.
7
8

9 3 S.F. Jordan^a, S.S. O'Reilly^b, D. Praeg^{c,d}, D. Dove^e, L. Facchin^d, R. Romeo^d, M. Szpak^f, X.
10 4 Monteys^f, B.T. Murphy^a, G. Scott^g, S.S. McCarron^g, and B.P. Kelleher^{a,*}
11
12
13
14

15 6 ^a *School of Chemical Sciences, Dublin City University, Dublin 9, Ireland*

16 7 ^b *Department of Earth, Atmospheric, and Planetary Sciences, Massachusetts Institute of*
17 8 *Technology, Cambridge, MA, USA*

18 9 ^c *Géoazur (UMR7329 CNRS), 250 Rue Albert Einstein, 06560 Valbonne, France*

19 10 ^d *OGS (Istituto Nazionale di Oceanografia e di Geofisica Sperimentale), Borgo Grotta Gigante*
20 11 *42C, Trieste, 34010, Italy*

21 12 ^e *British Geological Survey, The Lyell Centre, Research Avenue South, Edinburgh, EH14 4AP,*
22 13 *UK*

23 14 ^f *Geological Survey of Ireland, Beggars Bush, Haddington Road, Dublin, Ireland*

24 15 ^g *Maynooth University Department of Geography, Maynooth, Co. Kildare, Ireland*
25
26
27

28 17 *Corresponding author: *E-mail address:* brian.kelleher@dcu.ie (B.P. Kelleher).
29
30
31
32

33 19 **Abstract**
34
35
36
37
38

39 21 An integrated geophysical, geological, and geochemical investigation of seabed fluid venting
40 22 was carried out in upper Bantry Bay, a large marine inlet on the southwest coast of Ireland.
41 23 The results provide evidence of the seafloor venting of gas rich fluids, resulting in the formation
42 24 of a pockmark field identified here for the first time. The pockmarks occur in an area where
43 25 sub-bottom profiles provide evidence of chimney-like features interpreted to record upward
44
45
46
47
48
49
50
51
52
53
54
55
56
57
58
59
60

61
62
63 26 gas migration through Quaternary sediments to the seafloor. Three vibrocores up to 6 m long
64
65 27 were acquired in water depths of 24-34 m, two from the pockmark field and one from outside.
66
67 28 Methane of predominantly biogenic origin was quantified in all three cores by headspace
68
69 29 analysis of sediment sub-samples. Well-defined sulfate methane transition zones (SMTZs)
70
71 30 were observed in two of the cores, the shallowest (1.25 metres below sea floor (mbsf)) inside
72
73 31 the pockmark field and the other (3.75 mbsf) outside. It is likely that an SMTZ occurs at the
74
75 32 location of the third core, also within the pockmark field, although deeper than the samples
76
77 33 obtained during this study. Gas migration towards the seafloor is suggested to involve both
78
79 34 diffuse pore fluid migration across wide areas and focused flow through the pockmarks,
80
81 35 together driven by methanogenesis of pre-glacial lacustrine sediments preserved in a bedrock
82
83 36 basin, and possible gas release from the Owenberg River Fault. Analysis of phospholipid fatty
84
85 37 acids (PLFAs) and archaeal isoprenoid hydrocarbons was used to investigate the microbial
86
87 38 ecology of these sediments. Anaerobic oxidation of methane (AOM) may play a role in
88
89 39 controlling release of CH₄ to the water column and atmosphere in this shallow gas setting,
90
91 40 potentially mediated by syntrophic sulfate reducing bacteria (SRB) and anaerobic
92
93 41 methanotrophic archaea (ANME).
94
95
96
97
98
99

100 **Keywords**

101
102 44 Seafloor; pockmarks; biogeochemical processes; fluid migration; anaerobic oxidation of
103
104 45 methane (AOM); lipid biomarkers; methane; climate change; geohazards
105
106
107

108 **1. Introduction**

109
110
111
112 49 Pockmarks are concave depressions within seabed sediments, circular to ellipsoidal in
113
114 50 shape, ranging from <1 to 400 m in diameter and up to 20 m deep (Hovland and Judd, 1988;
115
116
117
118
119
120

121
122
123 51 King and MacLean, 1970), although typically 30 to 40 m wide and 2 to 3 m deep (Acosta et
124
125 52 al., 2001). Pockmarks can occur as singular features, in linear patterns known as pockmark
126
127 53 trains, or in complex groups known as pockmark fields. The formation and dynamics of these
128
129 54 features are still not fully understood, but they are generally considered to be the result of the
130
131 55 expulsion of fluids typically including hydrocarbon gases, mainly methane (CH₄), from
132
133 56 seafloor sediment (Hovland, 2013; Hovland and Judd, 1988). The emission of fluids containing
134
135 57 gas from pockmarks makes them of interest in relation to issues of global carbon cycling and
136
137 58 climate change, as well as for seafloor geohazards (Judd and Hovland 2007).

138
139
140 59 Geologic Emissions of Methane (GEM), which include marine seeps such as
141
142 60 pockmarks, have been recognized as a natural source of atmospheric methane second only to
143
144 61 wetlands (Etiope et al., 2008). As a greenhouse gas, the warming potential of CH₄ outweighs
145
146 62 carbon dioxide (CO₂) by a factor of 25 times per ton, and since pre-industrial times is estimated
147
148 63 to have been responsible for approximately 20% of the Earth's warming (Yvon-Durocher et
149
150 64 al., 2014). Recent work indicates that contributions from marine sources have been greatly
151
152 65 underestimated (Skarke et al., 2014) and there is a need for CH₄ flux revisions in terms of
153
154 66 understanding the global carbon cycle (Judd and Hovland, 2009). Seepage sites are globally
155
156 67 widespread in shallow water coastal regions and have been suggested to be an important source
157
158 68 of CH₄ (Borges et al., 2016; Janssen et al., 2005; Shakhova et al., 2010; Skarke et al., 2014).
159
160 69 However, global estimates of the contribution to atmospheric CH₄ concentrations from marine
161
162 70 seepage sites are highly uncertain (Römer et al., 2014).

163
164
165
166 71 The presence of pockmarks may also be of significance in terms of marine geohazards
167
168 72 (Hovland, 1989). Fluid migration through marine sediments, through its influence on pore
169
170 73 pressures and sediment strength, is thought to play a key role in slope failure and seabed
171
172 74 instability (e.g. Locat and Lee, 2002). Therefore in pockmarked areas the development of
173
174 75 offshore infrastructures, such as pipelines, may need to avoid these features (Hovland et al.,
175
176
177
178
179
180

181
182
183 76 2002). In addition, pockmarks have been suggested as possible indicators of seismic activity
184
185 77 (Hovland et al., 2002), based on observations of gas venting from pockmarks before and during
186
187 78 earthquakes at sites in California (Field and Jennings, 1987) and Greece (Hasiotis et al., 1996;
188
189 79 Soter, 1999). Large-scale multinational monitoring of pockmarks has been advocated (Hovland
190
191 80 et al., 2002).

194 81 Anaerobic oxidation of methane (AOM) and the microbial consortia involved are
195
196 82 important factors in the global methane cycle, and yet they are still poorly understood (Gauthier
197
198 83 et al., 2015; Ruff et al., 2016). Although large amounts of CH₄ are transported from deep
199
200 84 reservoirs to shallow sediments, it is estimated that <3% reaches the atmosphere due to the
201
202 85 AOM performed by microbial communities (Niemann and Elvert, 2008). The predominant
203
204 86 mechanism of AOM is thought to be a syntrophic process whereby anaerobic methanotrophic
205
206 87 archaea (ANME) and sulfate reducing bacteria (SRB) oxidise CH₄ to CO₂ whilst reducing
207
208 88 SO₄²⁻ to H₂S providing energy for both microbial consortia (Boetius et al., 2000; Elvert et al.,
209
210 89 2003; Reeburgh, 2007; Valentine and Reeburgh, 2000):



213 90
214
215 91 These communities are predominantly found in sediments, however they have also been
216
217 92 found in anoxic marine and saline lacustrine water bodies, and in terrestrial mud volcanoes
218
219 93 (Alain et al., 2006; Joye et al., 1999; Wakeham et al., 2003). AOM primarily occurs at what is
220
221 94 known as the sulfate methane transition zone (SMTZ), where CH₄ diffusion from deeper
222
223 95 sediments and SO₄²⁻ penetration from seawater provide optimal conditions for AOM
224
225 96 communities (Knittel and Boetius, 2009).

228 97 Lipid biomarkers can provide evidence for the role played by archaea and SRB in AOM
229
230 98 (Caldwell et al., 2008). Phospholipid fatty acids (PLFAs) are fatty acids chemically cleaved
231
232 99 from ester linkage to polar head groups and are a useful tool to provide quantitative measures
233
234 100 of viable biomass and microbial community composition (Ringelberg et al., 1997; Zelles,

241
242
243 101 1997). Phospholipids are rapidly degraded after cell death making them excellent biomarkers
244
245 102 for viable microbial cells (Navarrete et al., 2000; White et al., 1997). Certain PLFAs have been
246
247 103 used as chemotaxonomic markers for SRB, such as C_{16:1ω5c} and cyC_{17:0ω5,6} as indicators of
248
249 104 *Desulfosarcina/Desulfococcus* species (Elvert et al., 2003). Archaeal cell membranes are
250
251 105 comprised of ether-linked isoprenoid lipids (Schouten et al., 2013). Analysis of these intact
252
253 106 lipids or their hydrocarbon skeletons (e.g. phytane, acyclic and cyclic C₄₀ isoprenoids) in
254
255 107 environmental samples provides a broad measure of archaeal abundance and diversity (e.g.
256
257 108 (King et al., 1998). δ¹³C values of AOM derived lipids are typically significantly depleted with
258
259 109 values < -50‰ (Elvert et al., 2003; Niemann and Elvert, 2008; van Dongen et al., 2007).
260
261 110 Isolation of these compounds combined with determination of their δ¹³C signatures can help
262
263 111 provide an overview of the microbial consortia and their involvement in AOM within cold seep
264
265 112 environments (Ge et al., 2015; Pancost et al., 2000).

266
267
268
269 113 Pockmark and seepage sites have been reported and investigated at several sites around
270
271 114 the coast of Ireland and we are only beginning to understand the dynamics and ubiquity of
272
273 115 coastal methane cycling (Croker et al., 2005, O'Reilly et al., 2014, Szpak et al., 2012, and
274
275 116 Szpak et al., 2015). In this paper we present the first description of a pockmark field in the
276
277 117 shallow waters (<30 m) of upper Bantry Bay, on the west coast of Ireland. The aim of the study
278
279 118 is to characterise CH₄ migration associated with the pockmarks, based on core data acquired
280
281 119 during an Irish-led campaign in 2014. The results provide information on the source of the CH₄
282
283 120 and its relation to the microbial ecology of this area, as well as the possible causes of pockmark
284
285 121 formation at this site. Our findings contribute to an improved understanding of gas venting
286
287 122 features in Irish coastal waters, that may be relevant to environmental planning, economic
288
289 123 developments, and global climate change.

290
291
292
293
294
295 124

295 125 **2. Regional setting**

301
302
303 126
304
305 127
306
307
308 128
309
310 129
311
312 130
313
314 131
315
316 132
317
318 133
319
320 134
321
322 135
323
324 136
325
326 137
327
328 138
329
330 139
331
332 140
333
334 141
335
336 142
337
338 143
339
340 144
341
342 145
343
344 146
345
346 147
347
348 148
349
350 149
351
352 150
353
354
355
356
357
358
359
360

Bantry Bay is the largest marine inlet in the southwest of Ireland, spanning an offshore area of 300 km² (Fig. 1A). It is approximately 40 km long, narrowing in width from 10 km at its mouth, where water depths are up to 60 m, to 5 km at its head. The bay contains two large islands; Bere Island in the outer bay and Whiddy Island in the inner bay. The Melagh, Owvane, Coomhola, Glengarriff, and Adrigole rivers all drain into Bantry Bay. Geologically, the bay lies within the South Munster Basin, comprising Devonian strata dominated by the Old Red Sandstone beneath uppermost Devonian and Carboniferous marine sandstones and mudstones (Plets et al., 2015; Vermeulen et al., 2000). Several fault lines are inferred to run through the bay offsetting the Old Red Sandstone (Fig. 1B): the Bantry Fault runs from the southeast of Whiddy Island, continuing along the centre of the bay; the Owenberg River Fault lies north east of Whiddy Island before meeting the Bantry Fault; while northeast of Whiddy Island are the Glengarriff Harbour and Coolieragh Faults (Szapak et al., 2015).

The sedimentary infill of the Bay was described by (Plets et al. 2015), based on sub-bottom profiles tied to shallow sediment cores, who recognized bedrock to be overlain by up to six units, interpreted to record deposition prior to and since the last glacial maximum (LGM). The oldest unit corresponds to stratified sediments infilling bedrock depressions, correlated to pre-LGM lacustrine sediments reported in the upper Bay by Stillman (1968). This is overlain by glacial sediments, truncated by tidal to estuarine units recording the inundation of the Bay and capped by a seafloor unit recording the establishment of fully marine conditions after 11 ka BP. In the inner Bay, the upper stratified marine unit is underlain by a unit of strong discontinuous reflections described as ‘turbid’, that cores show to correspond to estuarine deposits, laminated sands and muds containing organic matter, suggested on the basis of its acoustic character to also contain pockets of gas (Plets et al. 2015). In addition, in the upper Bay above at least 65 m water depth, the sediment column is crossed by vertical, pillar-like

361
362
363 151 acoustic turbidity zones (ATZs) that rise to within several metres of seafloor; although not
364
365 152 interpreted by Plets et al. (2015), these appear typical of gas chimneys (Dondurur et al. 2011).

367 153 Seabed classification maps based on backscatter and particle size analysis (PSA) show
368
369 154 that the sediment type is predominantly mud to fine sand with increasing medium to coarse
370
371 155 sand towards the mouth of the bay. There are areas of medium to coarse sand, coarse sand to
372
373 156 gravel, and rock throughout the bay primarily along the perimeter (INFOMAR, 2011).

374
375
376 157

378 158 **3. Materials and methods**

379
380 159

381
382 160 The data used in this study were acquired during campaigns undertaken as part of the
383
384 161 INFOMAR (Integrated Mapping for the Sustainable Development of Ireland's Marine
385
386 162 Resources) programme. Acoustic datasets including multibeam bathymetric and backscatter
387
388 163 coverage of all of Bantry Bay were obtained during INFOMAR campaigns from 2004-2007
389
390 164 (see Plets et al. 2015), while the sediment cores and sub-bottom profiles used in this study were
391
392 165 acquired as part of the GATEWAYS campaign of the Celtic Explorer in February 2014
393
394 166 (CE14003).

395
396
397 167

398 399 168 *3.1. Acoustic data*

400
401 169 Seafloor bathymetric and backscatter data were collected using two Kongsberg Simrad
402
403 170 multibeam systems, an EM1002 (95 kHz) and an EM3002D (200 kHz). The multibeam data
404
405 171 were processed using QTC Multiview software to generate bathymetric terrain models of 2 x
406
407 172 2 m grid size. No multibeam water column data were available for this study.

408
409 173 Sub-bottom profiles were acquired in 2014 using a heave-corrected SES Probe 5000
410
411 174 pinger with a 4x4 transducer array (hull-mounted) and a CODA DA2000 acquisition system.

421
422
423 175 Frequency content of 2.5 kHz corresponds to decametric vertical resolution. Acquisition
424
425 176 parameters, data logging, and interpretation were performed using the CODA Geokit suite.
426
427
428 177

429 178 *3.2. Sediment cores*

431
432 179 Three sediment cores were obtained in 2014 using a 6 m pneumatic vibrocorer,
433
434 180 deployed in water depths of 24-34 m. Recorded positions are those of the ship, which may
435
436 181 differ from the corer by up to 30 m. Two cores were obtained from within the pockmark field
437
438 182 and one core was taken from outside the field. Once on deck, cores were cut into 1 m sections
439
440 183 and capped. Core sections were split and the archive halves were photographed and logged.
441
442 184 Sediment porewaters were sampled downcore using Rhizons (Rhizosphere Research Products)
443
444 185 for analysis of SO_4^{2-} distribution. These were attached to 10 mL plastic syringes to create
446
447 186 vacuum pressure. The sampled porewater was placed in a plastic vial and preserved with 10
448
449 187 μL CHCl_3 for sulfate analysis. All porewater samples were refrigerated at 4°C onboard for the
450
451 188 duration of the cruise and back in the laboratory prior to analysis.

452
453 189 Gas samples were immediately taken from the vibrocore sections to determine gas
454
455 190 composition and distribution. Two 10 cm³ sediment plugs were sampled using plastic syringes
456
457 191 with tips removed and transferred to 50 mL glass headspace vials containing 20 mL 2 M
458
459 192 sodium hydroxide. Vials were sealed, homogenised, and stored upside-down in the dark at 4
460
461 193 °C for the duration of the cruise.

462
463 194 Sediment sub-samples were taken immediately after porewater and gas sub-samples.
464
465 195 Particle size analysis (PSA) samples were placed in ziplock bags and stored at room
466
467 196 temperature. Samples for lipid biomarker analysis were wrapped in fired Al foil, placed in
468
469 197 ziplock bags, and stored at -20 °C.

472 198

474 199 *3.3. Porewater and gas analysis*

481
482
483 200 SO_4^{2-} concentration in porewater was determined by the turbidimetric method. 10 mL
484
485 201 of sample was stirred constantly and 2-3 drops of glycerol were added. Crushed BaCl_2 ,
486
487 202 approximately 50 mg, was added to the mixture and stirring was continued for 1 minute after
488
489 203 which an aliquot was taken and the absorbance measured at 420 nm on a Shimadzu UV Mini
490
491 204 1240. Further aliquots were taken after 2, 2.5, and 3 minutes and an average reading was
492
493 205 calculated and used to determine concentration by extrapolation from a calibration curve. The
494
495 206 calibration curve was prepared with Na_2SO_4 standards in a range of 10 to 100 ppm.

498 207 CH_4 analysis was performed on an Agilent 7820A GC-FID with a 30 m HP-PLOTQ
499
500 208 column (Agilent, Santa Clara, USA). Column conditions were isothermal (50 °C). CH_4 was
501
502 209 quantified using calibration standards prepared from a 99.995% CH_4 standard (Sigma Aldrich,
503
504 210 Dorset, UK).

506
507 211

508 212 *3.4. Bulk physical and chemical analysis*

509
510 213 PSA and total organic carbon (TOC) data were obtained from sub-samples taken
511
512 214 surrounding the SMTZ locations which were determined by CH_4 and SO_4^{2-} analyses. PSA was
513
514 215 determined by laser granulometry using a Mastersizer 2000 particle size analyser (Malvern,
515
516 216 Worcestershire, UK). Organic carbon (OC) was removed using 30% hydrogen peroxide (H_2O_2)
517
518 217 prior to analysis. Elemental analysis was performed in triplicate using a Fisons NCS 1500 NA
519
520 218 elemental analyser. Samples were treated with 1 N HCl in Ag capsules following the procedure
521
522 219 of Verardo et al. (1990) to remove carbonate. After drying overnight, the capsules were
523
524 220 wrapped in Sn boats and combusted in the presence of O_2 . The CO_2 evolved was measured and
525
526 221 the TOC content (%) calculated by comparison with the certified reference standard
527
528 222 acetanilide.

530
531 223

532 224 *3.5. Lipid biomarker analysis*

541
542
543 225 Sediment samples were selected from sub-samples associated with the SMTZs. These
544
545 226 were freeze-dried and homogenized and lipid compounds were extracted from 30 g of
546
547 227 powdered sediment using a modified Bligh-Dyer extraction (White et al., 1997). Total lipid
548
549 228 extracts (TLEs) were concentrated and elemental S was removed by reaction with activated
550
551 229 Cu. TLEs were fractionated into neutral, glyco-, and polar lipids using Bond-Elut SPE columns
552
553 230 packed with an aminopropylsilica solid phase (5mm diameter, PE, 500mg Ultra-Clean NH₂,
554
555 231 Agilent Technologies) as outlined by Pinkart et al. (1998). A portion of each polar lipid fraction
556
557 232 was subjected to acid methanolysis (0.5 M sodium methoxide, 50 °C, 30 min) to transmethylate
558
559 233 ester-linked fatty acids. Double-bond positions of monounsaturated PLFAs were determined
560
561 234 by the formation of dimethyl disulfide (DMDS) adducts as described by Nichols et al., (1986).
562
563 235 Archaeal isoprenoid lipids were separated from polar head groups by cleavage of their ether
564
565 236 linkages following the method of Trent et al. (2003). 100 ppm 5 α cholestane was added to all
566
567 237 derivatised fractions as an internal standard prior to analysis.

570
571 238 Aliquots (1 μ l) of samples were injected in triplicate onto an Agilent model 7890N gas
572
573 239 chromatograph coupled to an Agilent 5973N mass selective detector operating in electron
574
575 240 impact mode at 70 eV. The column was a 30 m HP-5MS column (0.25 mm i.d., 1 μ m film
576
577 241 thickness). Each sample (1 μ l) was injected with a 2:1 split ratio. The GC inlet temperature
578
579 242 was 280 °C and the oven programme was 65 °C (held 2 min) to 300 °C (held 20 min) at 6
580
581 243 °C/min. Individual compounds were assigned from comparison with mass spectral library
582
583 244 databases (NIST and Wiley) and comparison of MS patterns with published spectra and
584
585 245 authentic standards. Analytes were quantified from total ion peak area using multiple-point
586
587 246 calibration curves of representative standards (methyl tetradecanoate and squalane).
588
589 247 Percentage recovery was measured using an internal standard added prior to extraction and was
590
591 248 found to be > 95%. Procedural blanks were run to monitor background interferences.
592
593
594
595
596
597
598
599
600

601
602
603 249 1 μ l aliquots of samples were injected in triplicate onto an Agilent model 7890N gas
604
605 250 chromatograph coupled to an IsoPrime 100 isotope ratio mass spectrometer. The $\delta^{13}\text{C}$ values
606
607
608 251 were measured against a CO_2 reference gas of known $\delta^{13}\text{C}$ value and are reported vs. a stable
609
610 252 isotope reference standard (*n*-alkanes mixture B2, Indiana University, USA). Reproducibility
611
612 253 was better than $\pm 0.5\%$ and only well resolved major analytes are reported here.

614 254 Lipid nomenclature is according to $x\text{Cy}\omega z$, where *x* refers to the number of carbon
615
616 255 atoms present, *y* refers to the number of double bonds on the carbon chain and *z* refers to the
617
618 256 position of the first double bond from the methyl end. Iso and anteiso branching is denoted by
619
620 257 ‘*i*’ and ‘*ai*’ respectively whilst the presence of the cyclopropane ring in a compound is denoted
621
622 258 by ‘*cy*’.

623
624
625 259

626 627 260 **4. Results**

628
629 261

630 631 262 *4.1. Geophysical analyses*

632
633 263 Multibeam morpho-bathymetric data provide evidence of an elongate pockmark field
634
635 264 north of Whiddy Island (Fig. 2). This is a narrow (max width ca. 275 m) pockmark field of
636
637 265 approximately 2.4 km in length, covering an area of ca. 0.5 km². Interestingly, this field
638
639 266 coincides with part of the Owenberg River Fault (Fig. 1B). The data show that the pockmarks
640
641 267 average ca. 10 m in diameter and are of low relief, with some features near the core locations
642
643 268 as shallow as ca. 0.3 m in depth (Fig. 2B). Recorded GPS position onboard the vessel may
644
645 269 differ from the actual sample location by up to 20–30 m. Therefore, although both VC24 and
646
647 270 VC25 were taken within the pockmark field, it is not possible to be sure whether either core
648
649 271 penetrated directly into a single pockmark feature.

650
651
652 272 A sub-bottom profile for VC27 was not prepared as the data was obstructed by
653
654 273 sideswipe from a rocky outcrop. Sub-bottom profiles across the sites of VC24 and VC25

661
662
663 274 provide acoustic evidence of gas migration through the sediment column (Fig. 3). The
664
665 275 sedimentary succession is crossed by columnar or conical zones of blanking (AB on Fig. 3),
666
667 276 most of which underlie strong reflector segments that lie at varying depths of ca. 4-10 metres
668
669 277 below sea floor (mbsf) (Fig. 3). Similar ‘pillar-like’ acoustic zones were previously described
670
671 278 on sub-bottom profiles across upper Bantry Bay by Plets et al. (2015). On high frequency
672
673 279 seismic data, such effects may arise due to overlap with the resonance frequencies of gas bubble
674
675 280 populations, resulting in energy loss by attenuation (reverberation and scattering) as well as
676
677 281 changes in P-wave velocity (Mathys et al. 2005). Gas concentrations as low as 0.5% may result
678
679 282 in a range of possible amplitude and coherence effects described as acoustic turbidity (Abegg
680
681 283 and Anderson 1997; Fleischer et al. 2001; Judd and Hovland 2007). We interpret the vertical
682
683 284 acoustic zones observed in Bantry Bay to be typical chimney structures, recording the upward
684
685 285 migration of gas-rich fluids through the sediment column (e.g. Dondurur et al., 2011).

686
687 286 On Fig. 3, the tops of the chimneys are seen to lie at varying stratigraphic levels, the
688
689 287 shallowest within an interval of strong discontinuous reflections of varying thickness. This
690
691 288 interval corresponds to unit III of Plets et al. (2015), which their cores showed to comprise
692
693 289 organic-rich laminated sands/muds of estuarine origin, hypothesised to contain gas pockets due
694
695 290 to their acoustically ‘turbid’ character. This unit was also penetrated by our cores, which
696
697 291 provide no evidence that its acoustic character can be correlated to higher gas content. We
698
699 292 suggest instead that the reflective character is likely to reflect the unit’s distinctive lithology,
700
701 293 comprising sand and mud laminae capable of generating strong impedance contrasts (SI Fig.
702
703 294 S1).

704 295 705 706 296 *4.2. Gas and porewater geochemistry*

707
708 297 All measured CH₄ values are provided in the supporting information (SI Table S1). The
709
710 298 highest concentrations of CH₄ were observed in VC24, taken from the pockmark field (Fig. 4).

721
722
723 299 Values fluctuated between 2.62 and 3.57 mM rising through the core before steadily decreasing
724
725 300 from 3.28 mbsf (3.68 mM) to the surface sample at 0.01 mbsf (0.002 mM), the minimum
726
727 301 overall value for VC24. SO_4^{2-} concentrations for VC24 ranged from 7.0 to 26.8 mM displaying
728
729 302 an overall decreasing trend from the surface, opposite to that of CH_4 (Fig. 4). A minimum value
730
731 303 was observed at 2.12 mbsf from which concentrations remain relatively constant through to
732
733 304 the bottom of the core.

734
735
736 305 Overall CH_4 concentrations detected within VC25 were the lowest of the three
737
738 306 vibrocores analysed with a maximum observed at 5.23 mbsf (0.018 mM) and a minimum
739
740 307 observed at 1 mbsf (Fig. 4). Concentrations decrease gradually from the base of the core to the
741
742 308 sediment surface from 0.016 mM to 0.003 mM. Concentrations of porewater SO_4^{2-} were
743
744 309 relatively high throughout VC25 compared to VC24 and VC27 (Fig. 4). Values were gradually
745
746 310 depleted from the seafloor (0.17 mbsf) with a concentration of 22.1 mM to the deepest sample
747
748 311 from the core (5.66 mbsf) with a concentration of 12.0 mM.

749
750
751 312 In VC27, outside the pockmark field, CH_4 concentrations decreased from 3.66 mM at
752
753 313 the base of the core (4.96 mbsf) to 0.97 mM at 4.08 mbsf before falling sharply to 0.07 mM at
754
755 314 3.6 mbsf (Fig. 4). Depletion gradually continued from this depth to 0.001 mM at the surface of
756
757 315 the core (0.02 mbsf). SO_4^{2-} concentrations followed an opposing trend with a maximum of 23.9
758
759 316 mM at 0.02 mbsf decreasing to a minimum of 7.1 mM at 4.08 mbsf and remained at similar
760
761 317 concentration to the base (4.96 mbsf) (Fig. 4).

762
763 318

764 319 *4.3. PSA and elemental analysis*

765
766
767
768 320 The overall sediment type for the three cores taken from Bantry Bay was poorly to very
769
770 321 poorly sorted sandy mud. All values for mean particle size, percentage clay, silt, sand, and
771
772 322 gravel are provided in table 1. Mud percentages (clay and silt) ranged from 69.4 to 92.3% in
773
774 323 VC24, from 42.2 to 81.2% in VC25, and from 29.3 to 84.0% in VC27. The 42.2% value from
775
776
777
778
779
780

VC25 was obtained at 4.99 mbsf, a sample comprised of poorly sorted muddy sand due to its high sand content (57.8%). The 29.3% value in VC27 was obtained at 1.93 mbsf where sediment type can be described as very poorly sorted, slightly gravelly, muddy sand due to its gravel (4.9%) and sand (65.8%) content. This gravel-containing layer had the largest mean particle size of 0.8 phi whereas the lowest value of 5.3 phi was observed in VC24 at 0.77 mbsf, the layer with the highest overall mud content (92.3%). The mean particle size for the remaining samples ranged between 4.5 and 3.3 phi.

Total organic carbon (TOC) content was low throughout all cores with an average overall value of 0.6% (Table 2). The highest observed values were 2 and 1.2% for VC24 0.025 and 0.27 mbsf respectively. No other sample had a value greater than 0.7%. In VC24, TOC decreased from 0.025 to 1.93 mbsf (2 to 0.3%) before increasing slightly to 0.5% at 2.92 mbsf and decreasing again to 0.3% at 3.9 mbsf. VC25 values were relatively constant. The TOC content of VC27 at 1.93 and 2.96 mbsf was 0.5%. This decreased to 0.4% at 3.98 mbsf and 0.3% at 4.97 mbsf.

Table 1. PSA results for all vibrocores.

Core	Depth (mbsf)	Mean (phi)	Clay (%)	Silt (%)	Sand (%)	Gravel (%)
VC24	0.08	4.5	10.6	69.4	20	0
	0.33	3.3	10.1	62.8	27.1	0
	0.72	5.3	15.3	77	7.7	0
	1.88	4.0	9.7	68.9	21.4	0
	2.97	3.7	6.2	77.2	16.6	0
	3.96	3.8	5.5	63.9	30.6	0
VC25	0.81	3.7	2.3	63.5	34.2	0
	2.93	3.4	6.1	62.8	31.1	0
	3.93	4.3	8.4	72.7	18.8	0
	4.99	3.6	1.8	40.4	57.8	0
VC27	0.93	0.8	2.7	26.6	65.8	4.9
	1.96	4.1	11.9	72.1	16	0
	2.98	4.1	10.9	69.1	20	0

841
842
843
844
845 340
846
847 341
848
849 342
850
851 343
852
853 344
854
855 345
856
857 346
858
859 347
860
861 348
862
863 349
864
865 350
866
867 351
868
869 352
870
871 353
872
873 354
874
875 355
876
877 356
878
879 357
880
881 358
882
883 359
884
885 360
886
887 361
888
889 362
890
891 363
892
893
894
895
896
897
898
899
900

3.97	3.4	11.7	41	47.3	0
------	-----	------	----	------	---

4.4.4. Lipid biomarkers

A summary of key lipid biomarker concentrations is provided in table 2. The highest overall concentrations of PLFAs in all three vibrocores were observed in VC24. 310.1 and 235.2 $\mu\text{g gOC}^{-1}$ were detected at 0.03 and 0.27 mbsf respectively, the largest quantities of PLFAs in all analysed samples. The remaining depths of VC24 contained between 31.1 (0.77 mbsf) and 90.1 $\mu\text{g gOC}^{-1}$ (1.93 mbsf). Saturated fatty acids (SATFAs) and monounsaturated fatty acids (MUFAs) were the dominant PLFAs at 0.03 and 0.27 mbsf whilst SATFAs and branched fatty acids (brFAs) were dominant from 0.77 to 3.9 mbsf. Polyunsaturated fatty acids (PUFAs) were not found at 1.93 or 2.92 mbsf and were the smallest class of PLFAs at all other depths. Total PLFA concentrations ranged from 49.7 to 73.9 $\mu\text{g gOC}^{-1}$ (5.96 and 2.93 mbsf respectively) in VC25. SATFAs were the dominant compounds throughout the core with concentrations approximately 10 times greater than MUFAs and brFAs. There were no PUFAs observed in any VC25 samples. The highest concentration of PLFAs in VC27 was 77.4 $\mu\text{g gOC}^{-1}$ observed at 3.98 mbsf. The lowest concentration was 51.2 $\mu\text{g gOC}^{-1}$ which was observed at 1.93 mbsf. Similar to VC25, total SATFA concentrations were significantly greater than other PLFA classes. There was little variation in total concentrations of other PLFA classes throughout the core.

Five archaeal ether (AE) lipids were isolated from each sample taken from VC24, VC25, and VC27. These were; phytane, acyclic biphytane ($\text{cyC}_{40:0}$), and three cyclic biphytanes ($\text{cyC}_{40:1}$, $\text{cyC}_{40:2}$, and $\text{cyC}_{40:3}$). The $\text{cyC}_{40:0}$ was the major isoprenoid in all samples whilst the $\text{cy}_{40:1}$ was the minor isoprenoid.

4.5. Carbon isotope values of individual PLFAs

901
902
903 364 $\delta^{13}\text{C}$ values could not be obtained for most lipid compounds identified in the three
904
905 365 Bantry Bay vibrocores. This was due to a combination of low abundance in polar lipid extracts
906
907
908 366 and low sensitivity of the GC-IRMS instrument. $\delta^{13}\text{C}$ values for three PLFAs were measured
909
910 367 in the VC24 0.27 sample which contribute to the study of these sediments. The MUFAs $\text{C}_{16:1\omega7}$
911
912 368 and $\text{C}_{16:1\omega5}$ provided $\delta^{13}\text{C}$ values of -31.0‰ and -46.1‰ respectively, and the SATFA $\text{C}_{16:0}$
913
914 369 $\delta^{13}\text{C}$ value was -27.7‰.
915
916
917
918
919
920
921
922
923
924
925
926
927
928
929
930
931
932
933
934
935
936
937
938
939
940
941
942
943
944
945
946
947
948
949
950
951
952
953
954
955
956
957
958
959
960

961
 962
 963 370 Table 2. TOC values (%) and Biomarker concentrations ($\mu\text{g gOC}^{-1}$) for each vibrocore taken in Bantry Bay. Total overall concentrations
 964
 965
 966 371 and total concentrations for certain groups of biomarkers are included (indicated by the prefix Σ). Individual concentrations of selected
 967
 968 372 biomarker compounds from within each group are also shown. Depth in mbsf.

	VC24						VC25				VC27			
Depth	0.025	0.270	0.768	1.933	2.920	3.895	2.930	3.925	4.980	5.960	1.930	2.960	3.980	4.970
TOC	2.0	1.2	0.6	0.3	0.5	0.3	0.3	0.3	0.3	0.3	0.5	0.5	0.4	0.3
Σ PLFA	310.14	235.24	31.07	90.12	51.21	44.02	73.90	57.15	56.90	49.68	51.24	68.89	77.36	63.01
Σ SATFA	133.28	118.72	20.43	64.94	33.06	30.99	52.11	41.72	42.73	43.24	36.15	42.50	50.35	46.84
Σ MUFA	91.12	51.97	2.61	2.25	3.40	1.94	5.18	3.86	1.35	8.54	4.22	5.89	5.99	5.78
Σ PUFA	12.92	17.73	0.00	0.00	0.00	1.16	0.00	0.00	0.00	0.00	1.15	1.66	1.73	0.00
Σ brFA	64.58	32.62	4.31	4.44	12.15	7.62	7.19	5.09	5.17	4.38	4.91	4.90	4.50	5.25
Σ AE	4.67	5.40	7.39	13.37	19.30	11.75	11.35	4.25	9.18	6.93	11.20	10.28	9.37	5.98
SATFA														
12:0	0.78	0.65	0.10	-	-	-	0.25	-	0.19	-	0.16	0.14	0.18	-
13:0	0.35	0.27	0.05	-	-	-	0.07	-	0.08	-	0.11	0.13	0.12	0.11
14:0	7.34	6.85	1.36	0.98	1.43	0.94	2.00	1.06	1.60	1.12	1.81	1.82	1.58	1.78
15:0	2.69	2.27	0.63	0.54	0.77	0.54	0.82	0.60	0.73	0.61	0.91	0.83	0.63	0.71
16:0	28.08	20.90	6.38	5.77	8.21	5.73	8.65	7.04	6.14	7.29	8.32	6.46	8.03	8.82
17:0	2.52	1.16	0.33	0.47	1.58	0.40	0.53	0.52	0.46	0.53	0.52	0.62	0.57	0.65
18:0	10.40	2.49	1.75	2.55	3.68	2.30	3.32	2.89	3.53	3.09	2.69	3.48	3.97	4.33
19:0	2.70	5.54	0.28	0.50	0.56	0.93	0.71	0.90	0.51		0.60	0.62	0.73	0.76
MUFA														
16:1 ω ?	16.26	4.27	0.32	0.39	0.48	0.41	0.35	0.37	0.40	0.31	0.36	0.44	0.47	0.54

1002
1003
1004
1005
1006
1007
1008
1009
1010
1011
1012
1013
1014
1015
1016
1017
1018
1019
1020
1021
1022
1023
1024
1025
1026
1027
1028
1029
1030
1031
1032
1033
1034
1035
1036
1037
1038
1039
1040
1041
1042

16:1 ω 7	2.67	0.88	-	-	-	-	-	-	-	-	-	-	-	-	-
16:1 ω 5	5.72	2.40	0.19	-	-	-	-	-	-	-	-	0.21	0.20	-	-
18:1 ω 9	12.09	0.83	0.48	1.28	0.73	1.00	0.92	0.99	0.95	1.25	0.91	0.98	0.67	0.78	-
18:1 ω 7	24.80	9.96	0.40	0.59	0.41	-	-	-	-	-	0.45	-	0.84	0.86	-
19:1 ω ?	10.61	3.05	1.22	4.46	1.78	1.09	3.91	2.50	2.90	-	2.29	4.27	4.01	3.60	-
PUFA															
18:2 ω ?	-	-	-	-	-	-	-	-	-	-	-	0.44	0.56	0.67	-
20:4 ω 6	3.77	3.05	-	-	-	-	-	-	-	-	-	-	-	-	-
20:5 ω 3	3.71	5.54	-	-	-	-	-	-	-	-	-	-	-	-	-
brFA															
<i>i</i> 13:0	0.43	0.24	0.06	-	-	-	0.09	-	0.06	-	0.10	0.10	0.07	-	-
<i>ai</i> 13:0	0.58	0.40	0.05	-	-	-	0.13	-	0.08	-	0.16	0.15	0.10	-	-
<i>i</i> 15:0	7.68	3.37	0.47	0.61	0.77	0.75	0.79	0.55	0.53	0.45	0.63	0.66	0.55	0.60	-
<i>ai</i> 15:0	14.39	7.55	0.90	1.17	0.54	0.54	1.69	1.12	1.24	1.17	1.56	1.41	1.14	1.21	-
3Me15:0	-	-	-	-	-	-	0.25	-	-	-	0.29	0.52	0.35	0.36	-
<i>i</i> 16:0	3.18	2.40	-	-	-	0.53	0.70	0.78	-	-	0.56	0.67	0.51	0.47	-
<i>i</i> 17:0	2.13	1.36	0.18	0.43	0.27	0.38	0.29	0.32	0.39	0.85	0.30	0.29	0.27	0.26	-
<i>ai</i> 17:0	1.72	2.46	0.28	0.56	0.34	0.40	0.50	0.39	0.47	0.53	0.47	0.50	0.41	0.40	-
cyFA															
<i>cy</i> 17:0	-	4.36	-	-	-	-	-	-	-	-	-	-	-	-	-
AE															
Phytane	0.76	0.64	0.72	1.43	1.63	0.86	1.24	0.47	0.85	0.81	0.94	1.51	1.30	0.98	-
C40:0	2.28	2.72	3.47	5.80	8.25	4.75	5.04	1.79	4.24	3.19	5.62	4.40	4.26	2.95	-
C40:1	0.36	0.51	0.44	1.67	1.74	1.44	0.92	0.45	0.71	0.51	0.81	0.76	0.75	0.31	-

1043
1044
1045
1046
1047
1048
1049
1050
1051
1052
1053
1054
1055
1056
1057
1058
1059
1060
1061
1062
1063
1064
1065
1066
1067
1068
1069
1070
1071
1072
1073
1074
1075
1076
1077
1078
1079
1080
1081
1082
1083

C40:2	0.70	0.81	1.45	2.31	3.69	2.50	2.20	0.88	1.74	1.23	2.03	1.86	1.41	0.88
C40:3	0.57	0.72	1.31	2.16	3.99	2.21	1.94	0.67	1.64	1.19	1.79	1.75	1.65	0.87

1084
1085
1086 374 **5. Discussion**
1087

1088 375 Methane is widespread within upper Bantry Bay, as shown here through both
1089
1090 376 acoustic evidence and millimolar concentrations of CH₄ in core samples. Migration of
1091
1092 377 gas-rich fluids towards the seafloor is interpreted to have led to the formation of
1093
1094 378 pockmarks, which we describe here for the first time. Detailed geochemical analysis
1095
1096 379 of porewater samples coupled to results from the gas analysis of sediment plugs, depict
1097
1098 380 strong SMTZs occurring in two of three sediment core locations. Results from the
1099
1100 381 third core, VC25, suggest that a similar SMTZ likely occurs below the maximum
1101
1102 382 penetration depth of the vibrocorer. Lipid biomarker analysis provides evidence of the
1103
1104 383 presence of active communities of both SRB and archaea within these sediment cores.
1105
1106 384 These archaea are potentially anaerobic methanotrophs (ANME) which are likely
1107
1108 385 involved in AOM, contributing to the prevention of regular methane seepage above
1109
1110 386 the seafloor as evidenced by the distinct SMTZs.
1111
1112
1113

1114 387 Sub-bottom profiles provide evidence of vertical gas migration through the
1115
1116 388 sediments of upper Bantry Bay, although no gas signals were observed within the
1117
1118 389 water column, geochemical data provide evidence of low concentrations of gas just
1119
1120 390 beneath the seafloor. In the area of the pockmark field where our sediment cores were
1121
1122 391 obtained, we observed vertical zones of acoustic blanking (AB) beneath strong
1123
1124 392 reflectors at varying depths below the seafloor, which we interpret as typical gas
1125
1126 393 chimneys (Fig. 3). The observation of chimney-like features as well as of blanking
1127
1128 394 below enhanced reflectors suggest upward fluid migration is predominant at this
1129
1130 395 location (Szpak et al., 2012). Similar acoustic chimneys were observed to rise to within
1131
1132 396 a few metres of the seafloor across upper Bantry Bay above water depths of at least
1133
1134 397 65 m by Plets et al. (2015, their Fig. 10a), which we interpret to indicate the upward
1135
1136 398 migration of gas from depth over wide areas beneath the pockmark field. However,
1137
1138
1139
1140
1141
1142
1143

1144
1145
1146 399 our results do not support the suggestion of Plets et al. (2015) that the presence of gas
1147
1148 400 may account for the reflective character of their unit III, penetrated by our cores at ca.
1149
1150 401 2-6 mbsf (Fig. 3), which we instead suggest is due to its laminated lithological
1151
1152 402 character (SI Fig. S1).

1153
1154
1155 403 All gas headspace samples yielded undetectable amounts of C₂-C₄
1156
1157 404 hydrocarbons, indicating a biogenic source, rather than thermogenic source for gas in
1158
1159 405 Bantry Bay (Faber and Stahl, 1984; Floodgate and Judd, 1992). The likely origins of
1160
1161 406 this biogenic gas are microbial decomposition of buried organic matter and
1162
1163 407 methanogenesis (Antler et al., 2014; Froelich et al., 1979). River run-off likely delivers
1164
1165 408 a significant amount of OM to the bay. However, the majority of this terrestrially
1166
1167 409 derived OM is likely consumed in the surface sediments as seen from the TOC results
1168
1169 410 obtained from VC24. As such, this OM is probably not a large contributor to CH₄
1170
1171 411 generation within Bantry Bay. Previous work in Bantry Bay encountered black
1172
1173 412 lacustrine sediments at ca. 57 m water depth (ca. 25 mbsf) which were dated to 13-14
1174
1175 413 ka cal. BP within a borehole off Whiddy Island (Stillman, 1968). Plets et al. (2015)
1176
1177 414 found that these deposits occurred within Unit 2 of their assigned seismo-stratigraphy
1178
1179 415 profile. They suggested that the material was likely older than the value provided by
1180
1181 416 Stillman (1968) as they were situated below acoustic Unit 4 which was described as a
1182
1183 417 possible glacial till, thereby placing Unit 2 in the position of a pre-Last Glacial
1184
1185 418 Maximum (LGM) deposit. The LGM is defined as 26.5-19 ka BP (Clark et al., 2009).
1186
1187 419 These sediments likely undergo enhanced anaerobic decomposition and methanogenic
1188
1189 420 activity due to their high organic content which makes them favourable candidates for
1190
1191 421 the source of the gas observed in this area, however this awaits further investigation.
1192
1193

1194
1195 422 The pockmark field north of Whiddy Island is comprised of very shallow
1196
1197 423 depressions of ca. 0.3 m depth. Due to the substantial gas activity observed in these
1198
1199
1200
1201
1202
1203

1204
1205
1206 424 sediments it is likely that biogenic CH₄ resulting from the decomposition of organic
1207
1208 425 material, possibly from ancient lacustrine deposits buried deep beneath the seafloor,
1209
1210 426 was the primary cause of pockmark formation. Although no active seepage from
1211
1212
1213 427 pockmarks to the water column was observed in this study it is still possible that some
1214
1215 428 of them are actively venting. Wheeler (2002) determined that significant currents
1216
1217 429 regularly resuspend the seabed near Whiddy island. If the pockmarks were inactive,
1218
1219 430 this could suggest that they have been filled in by fresh sediment. However, recent
1220
1221 431 work suggests that inactive pockmarks can in fact be kept open by ocean currents
1222
1223 432 (Hammer et al., 2009; Pau et al., 2014). Many studies have proposed that accumulation
1224
1225 433 of large volumes of gas below the seafloor followed by periodic large expulsions is
1226
1227 434 the predominant cause of pockmark formations (Cole et al., 2000; Dondurur et al.,
1228
1229 435 2011; Gay et al., 2007; Hovland et al., 2002; Hovland and Judd, 1988). As such, these
1230
1231 436 events likely reform the present features in Bantry Bay and potentially form new
1232
1233 437 features as well. Further bathymetric analysis of this site is required to determine the
1234
1235 438 precise layout of this field and the exact number of pockmarks within it, as well as
1236
1237 439 regular monitoring of this area to determine the level of gas seepage activity which
1238
1239 440 may represent a potential hazard to any planned economic activity in the bay.

1242 441 A pockmark field in a similar setting has been described in Dunmanus Bay,
1243
1244 442 south of Bantry Bay (Szpak et al., 2015). These authors showed that the pockmarks
1245
1246 443 were associated with CH₄ emissions and argued that the source of the gas was an
1247
1248 444 underlying Dunmanus Fault, via a venting mechanism involving seal failure-renewal
1249
1250 445 cycles. The CH₄ from Dunmanus contained only trace levels of C₂-C₄ hydrocarbons
1251
1252 446 and it was suggested that methanogenesis also contributed to the gas in this location.
1253
1254 447 The Bantry Bay pockmark field overlies the Owenberg River Fault, which runs along
1255
1256 448 the northwest of Whiddy Island. It is possible that venting in Bantry Bay is controlled
1257
1258
1259
1260
1261
1262
1263

1264
1265
1266 449 by a similar bedrock faulting mechanism as proposed in Dunmanus. Both bays lie in
1267
1268 450 the South Munster Basin and are similar in their geology (Vermeulen et al., 2000).
1269
1270 451 However, a higher contribution of low molecular weight hydrocarbons would be
1271
1272 452 expected if this gas was predominantly thermogenic. Therefore, it is most likely that
1273
1274 453 the gas observed at both of these sites is a combination of thermogenic gas release
1275
1276 454 from underlying faults and biogenic gas produced by methanogenic communities
1277
1278 455 feeding on deeply buried organic material.

1281 456 Both VC24 and VC27 yielded clear SMTZs, where CH₄ diffusing upwards
1282
1283 457 from depth first encounters SO₄²⁻ diffusing downwards from the ocean, which reflect
1284
1285 458 the depth of maximal anaerobic oxidation (Antler et al., 2014; Lin et al., 2016;
1286
1287 459 Valentine, 2002). The decreasing trend of SO₄²⁻ in VC25 suggests complete depletion
1288
1289 460 coinciding with a SMTZ at ca. 10 mbsf. The sub-bottom profile suggests that there is
1290
1291 461 no significant gas penetration into this core whereas there is gas penetration observed
1292
1293 462 in the core location of VC24. This is consistent with the significantly lower CH₄
1294
1295 463 concentrations within the VC25 samples. Analysis of sediments from the deeper
1296
1297 464 SMTZ in VC25 would likely yield similar CH₄ concentrations to that of VC24 and
1298
1299 465 VC27. Thus the three cores are indicative of variable rates of upward penetration of
1300
1301 466 gas-rich fluids towards the seafloor.

1304 467 These SMTZs suggest that microbial communities are consuming CH₄ rising
1306
1307 468 from depth as well as SO₄²⁻ diffusing downward from the seafloor above. This
1308
1309 469 signature represents the metabolic pathways of microorganisms involved in the AOM,
1310
1311 470 namely ANME and SRB. At present, it appears that the activity of these microbial
1312
1313 471 communities aids in preventing the release of CH₄ to the water column and potentially
1314
1315 472 the atmosphere on a regular basis, reducing the potential impact of this powerful
1316
1317 473 greenhouse gas on global climate. However, as previously mentioned, the pockmark
1318
1319
1320
1321
1322
1323

1324
1325
1326 474 features are indicative of possible recurring episodic expulsions of gas from these
1327
1328 475 sediments and as such the overall CH₄ flux from this site is poorly constrained. This
1329
1330 476 is a scenario which is observed in shallow marine seepage environments around the
1331
1332 477 world. It is important for these unique environments to be monitored so that their
1333
1334 478 potential contribution to climate change can be better understood.
1335
1336

1337 479 PLFA biomarker results provide further evidence of this ongoing microbial
1338
1339 480 activity. High levels of MUFAs and low levels of PUFAs are an indication of the
1340
1341 481 dominant contribution of bacterial communities to sediment biomass (Rajendran et al.,
1342
1343 482 1995, 1992; Taylor and Parkes, 1983; Volkman et al., 1980). Bacteria appear to
1344
1345 483 dominate the microbial ecology in all three vibrocores in this study. Abundances of
1346
1347 484 PUFAs are increased in the surface sediments of VC24, however MUFA abundances
1348
1349 485 are still higher. Interestingly, at 0.8 and 3.9 mbsf in VC24, contributions of MUFAs
1350
1351 486 and PUFAs are similar although MUFAs remain dominant. Comparison of MUFAs
1352
1353 487 (<C₁₉) with total brFAs provides an insight to the aerobic/anaerobic conditions in the
1354
1355 488 sediment. Values less than 1 indicate an anaerobic environment whereas values greater
1356
1357 489 than 1 are representative of aerobic conditions (Rajendran et al., 1992). Only the
1358
1359 490 shallower sediments of VC24 (1.12 and 1.08 for 0.03 and 0.27 mbsf respectively) are
1360
1361 491 classified as aerobic using this approach, therefore the overall conditions observed
1362
1363 492 here are anaerobic.
1364
1365

1366 493 Mid-chain brFAs in marine sediments are often produced by SRB and are used
1367
1368 494 as chemotaxonomic markers for these microorganisms (Dowling et al., 1986; Li et al.,
1369
1370 495 2007). *iC*_{15:0}, *aiC*_{15:0}, *iC*_{16:0}, *iC*_{17:0}, and *aiC*_{17:0} are all reported biomarkers for the
1371
1372 496 *Desulfovibrio* species of SRB (Dowling et al., 1986; Findlay et al., 1990; Li et al.,
1373
1374 497 2007; Rajendran et al., 1995; Taylor and Parkes, 1983). These compounds were
1375
1376 498 present throughout all three vibrocores taken in Bantry Bay, suggesting a significant
1377
1378
1379
1380
1381
1382
1383

1384
1385
1386 499 contribution of SRB to the microbial ecosystem here. SRB tend to display a higher
1387
1388 500 ratio of *iC*_{15:0} to *aiC*_{15:0} in their PLFA profiles (Dowling et al., 1986). Applying this
1389
1390 501 ratio to the Bantry Bay sediments resulted in substantially higher values observed in
1391
1392 502 VC24 than VC25 or VC27, both of which had similar values. This suggests that SRB
1393
1394 503 are substantially higher contributors to the microbial community of VC24. Elvert et al
1395
1396 504 determined that *C*_{16:1 ω 5}, *C*_{17:1 ω 6}, and *cyC*_{17:0 ω 5,6} were specific membrane fatty acids for
1397
1398 505 SRB of the *Desulfosarcinia/Desulfococcus* group which were involved in AOM
1400
1401 506 (Elvert et al., 2003). *C*_{16:1 ω 5} was identified in four samples from the Bantry Bay
1402
1403 507 vibrocores; VC24 0.03 mbsf, VC24 0.27 mbsf, VC27 1.93 mbsf, and VC27 2.96 mbsf.
1404
1405 508 Isotope ratio analysis provided a depleted $\delta^{13}\text{C}$ value of -46.1‰ for this compound at
1406
1407 509 0.27 mbsf in VC24, compared with those obtained from more ubiquitous bacterial
1408
1409 510 PLFAs; 16:1 ω 7 and 16:0 at -31.0‰ and -27.7‰ respectively. While lipid abundances
1410
1411 511 are low, these depleted values still indicate the possible incorporation of CH₄ derived
1412
1413 512 C into the membranes of these SRB providing evidence of their involvement in AOM
1414
1415 513 at this site.

1418
1419 514 Archaeal biomarkers are present at all depths in all three vibrocores taken in
1420
1421 515 Bantry Bay. Archaea involved in AOM typically belong to three major anaerobic
1422
1423 516 methanotroph (ANME) consortia (Caldwell et al., 2008). It is generally assumed that
1424
1425 517 ANMEs oxidize and assimilate CH₄, following which CH₄-derived C is consumed by
1426
1427 518 the SRB as CO₂ or a partially oxidized intermediate completing the syntrophic reaction
1428
1429 519 (Alperin and Hoehler, 2009). It has been suggested that C₂₀ isoprenoids derived from
1430
1431 520 archaeal ether lipids may be specific biomarkers for ANME-2 archaea whilst C₄₀
1432
1433 521 isoprenoids may be specific for the ANME-1 type (Blumenberg et al., 2004; Brocks
1434
1435 522 and Pearson, 2005). The presence of these compounds within the gas-rich sediments
1436
1437 523 in Bantry Bay further suggests the involvement of AOM mediated by ANME and SRB

1444
1445
1446 524 in limiting gas release at this site. More detailed biogeochemical analysis of these
1447
1448 525 sediments could shed more light on the composition of this particular microbial
1449
1450 526 community with isotopic analysis determining their contribution to AOM. Due to the
1451
1452 527 importance of understanding the microbial community structure at shallow gas
1453
1454 528 seepage sites like Bantry Bay, a more detailed phylogenetic study of this site is
1455
1456 529 recommended.

1458
1459 530

1460
1461 531 **6. Conclusions**

1462
1463 532

1464
1465 533 The upward migration of gas-rich fluids through the sediment column appears
1466
1467 534 to be widespread in upper Bantry Bay, as inferred from chimney-like acoustic zones
1468
1469 535 on sub-bottom profiles and confirmed by shallow SMTZs within sediment cores.
1470
1471 536 Shallow SMTZs are observed both within and outwith a newly identified pockmark
1472
1473 537 field, suggesting that diffuse pore fluid upwelling over wide areas is only locally
1474
1475 538 accompanied by focused flow within conduits. Methanogenesis is taking place within
1476
1477 539 organic-rich Quaternary sediments deposited across the upper Bay prior to and since
1478
1479 540 the last deglaciation. The presence of pockmarks off Whiddy Island may be explained
1480
1481 541 by enhanced gas flux from the underlying Owenberg River Fault and methanogenesis
1482
1483 542 of organic-rich lacustrine sediments pre-dating the LGM that are preserved in bedrock
1484
1485 543 basins.

1486
1487 544 Fluid flow affects not only the physical nature of the sea-floor in the bay but
1488
1489 545 also the microbial ecosystem. The gas is CH₄ with a predominantly biogenic signature.
1490
1491 546 As CH₄ flows upwards from its origin it provides a substrate for certain
1492
1493 547 microorganisms to thrive in the shallower sediments above. Archaea, possibly
1494
1495 548 ANMEs, are present in these shallower sediments as are SRB. The CH₄ is steadily

1504
1505
1506 549 depleted before it reaches the seafloor and SO_4^{2-} concentrations also become depleted
1507
1508 550 in the opposite direction providing a well-defined SMTZ. This is likely due to AOM
1509
1510 551 carried out by these two groups of microorganisms in a syntrophic relationship,
1511
1512 552 however further work is needed to confirm this pathway. This study suggests that
1513
1514 553 AOM in Bantry Bay is important in limiting CH_4 emissions from the seafloor
1515
1516 554 preventing the potential climatic implications of a release of this powerful greenhouse
1517
1518 555 gas to the atmosphere. Similar conditions have been observed in a pockmark field in
1519
1520 556 Dunmanus Bay, to the east of Bantry Bay (Szpak et al. (2015)) and on the Malin Shelf
1521
1522 557 off the north coast of Ireland (Szpak et al. (2012)). This indicates that marine CH_4
1523
1524 558 production may be common around the island of Ireland.
1525
1526

1527
1528 559 Global estimates of the contribution of CH_4 from marine seepage sites are
1529
1530 560 highly uncertain (Römer et al., 2014). Release of CH_4 to the atmosphere has been
1531
1532 561 observed in Arctic regions, areas particularly vulnerable to climate change, and these
1533
1534 562 releases have been attributed to rising temperatures (Shakhova et al., 2010; Westbrook
1535
1536 563 et al., 2009). As CH_4 is a potent greenhouse gas, these releases serve only to increase
1537
1538 564 rates of global climate change. AOM and the microbial consortia involved are
1539
1540 565 important factors in the global methane cycle (Gauthier et al., 2015). For these reasons
1541
1542 566 further study of these sites and their microbial ecology should be prioritised.
1543
1544

1545 567

1546 568 **Acknowledgements**

1547
1548
1549 569

1550
1551 570 The authors would like to thank the INFOMAR program, joint programme
1552
1553 571 between the Geological Survey Ireland and the Marine Institute funded by DCCAE.
1554
1555 572 We also thank the captain and crew of the R.V. *Celtic Explorer* during the
1556
1557 573 GATEWAYS II campaign (CE14003), which was funded by a ship-time award to
1558
1559
1560
1561
1562
1563

1564
1565
1566 574 Stephen McCarron under the Sea Change strategy with the support of the Marine
1567
1568 575 Research Sub-programme of the Irish National Development Plan 2007-2013. We
1569
1570 576 would like to thank the Irish Research Council for supporting the work of those
1571
1572 577 researchers based at Dublin City University. The participation of OGS in the
1573
1574 578 GATEWAYS II campaign was supported by Italian PNRA project IPY GLAMAR
1575
1576 579 (grant number 2009/ A2.15), and Daniel Praeg also acknowledges funding from the
1577
1578 580 European Union's Horizon 2020 research and innovation program under the Marie
1579
1580 581 Skłodowska-Curie grant agreement No 656821 (project SEAGAS, 2016-2020). Bulk
1581
1582 582 physical analyses of core samples was carried out at the Coastal and Marine Research
1583
1584 583 Centre (CMRC) at University College Cork (UCC). We also thank Dr. Bart van
1585
1586 584 Dongen and the anonymous reviewers whose input significantly improved this
1587
1588 585 manuscript.
1589
1590
1591
1592
1593

1594 587 **References**

- 1595 588
1596
1597
1598 589 Abegg, F. & Anderson, A.L. 1997. The acoustic turbid layer in muddy sediments of
1599
1600 590 Eckernförde Bay, Western Baltic: methane concentration, saturation and bubble
1601
1602 591 characteristics. *Marine Geology*, 137, 137–147.
1603
1604 592 Acosta, J., Munoz, A., Herranz, P., Palomo, C., Ballesteros, M., Vaquero, M.,
1605
1606 593 Uchupi, E., 2001. Pockmarks in the Ibiza Channel and western end of the
1607
1608 594 Balearic Promontory (western Mediterranean) revealed by multibeam mapping.
1609
1610 595 *Geo-Marine Lett.* 21, 123–130.
1611
1612 596 Alain, K., Holler, T., Musat, F., Elvert, M., Treude, T., Krüger, M., 2006.
1613
1614 597 Microbiological investigation of methane- and hydrocarbon-discharging mud
1615
1616 598 volcanoes in the Carpathian Mountains, Romania. *Environ. Microbiol.* 8, 574–
1617
1618
1619
1620
1621
1622
1623

- 1624
1625
1626 599 90.
1627
1628 600 Alperin, M.J., Hoehler, T.M., 2009. Anaerobic methane oxidation by
1629
1630
1631 601 archaea/sulfate-reducing bacteria aggregates: 2. Isotopic constraints. *Am. J. Sci.*
1632
1633 602 309, 958–984.
1634
1635 603 Antler, G., Turchyn, A. V., Herut, B., Davies, A., Rennie, V.C.F., Sivan, O., 2014.
1636
1637 604 Sulfur and oxygen isotope tracing of sulfate driven anaerobic methane
1638
1639 605 oxidation in estuarine sediments. *Estuar. Coast. Shelf Sci.* 142, 4–11.
1640
1641 606 Blumenberg, M., Seifert, R., Reitner, J., Pape, T., Michaelis, W., 2004. Membrane
1642
1643 607 lipid patterns typify distinct anaerobic methanotrophic consortia. *Proc. Natl.*
1644
1645 608 *Acad. Sci.* 101, 11111–11116.
1646
1647 609 Boetius, A., Ravensschlag, K., Schubert, C.J., Rickert, D., Widdel, F., Gieseke, A.,
1648
1649 610 Amann, R., Jørgensen, B.B., Witte, U., Pfannkuche, O., 2000. A marine
1650
1651 611 microbial consortium apparently mediating anaerobic oxidation of methane.
1652
1653 612 *Nature* 407, 623–6.
1654
1655 613 Borges, A. V., Champenois, W., Gypens, N., Delille, B., Harlay, J., 2016. Massive
1656
1657 614 marine methane emissions from near-shore shallow coastal areas. *Sci. Rep.* 6,
1658
1659 615 27908.
1660
1661 616 Brocks, J.J., Pearson, A., 2005. Building the Biomarker Tree of Life. *Rev. Mineral.*
1662
1663 617 *Geochemistry* 59, 233–258.
1664
1665 618 Caldwell, S.L., Laidler, J.R., Brewer, E.A., Eberly, J.O., Sandborgh, S.C., Colwell,
1666
1667 619 F.S., 2008. Anaerobic Oxidation of Methane: Mechanisms, Bioenergetics, and
1668
1669 620 the Ecology of Associated Microorganisms. *Environ. Sci. Technol.* 42, 6791–
1670
1671 621 6799.
1672
1673 622 Clark, P.U., Dyke, A.S., Shakun, J.D., Carlson, A.E., Clark, J., Wohlfarth, B.,
1674
1675 623 Mitrovica, J.X., Hostetler, S.W., McCabe, A.M., 2009. The Last Glacial
1676
1677
1678
1679
1680
1681
1682
1683

- 1684
1685
1686
1687 624 Maximum. *Science* (80). 325, 710 LP – 714.
- 1688
1689 625 Cole, D., Stewart, S. a., Cartwright, J. a., 2000. Giant irregular pockmark craters in
1690
1691 626 the Palaeogene of the Outer Moray Firth Basin, UK North Sea. *Mar. Pet. Geol.*
1692
1693 627 17, 563–577.
- 1694
1695 628 Croker, P.F., Kozachenko, M., Wheeler, A.J., 2005. Gas-Related Seabed Structures
1696
1697 629 in the Western Irish Sea (IRL-SEA6), SEA6 Technical Report
- 1698
1699 630 Dondurur, D., Çifçi, G., Drahor, M.G., Coşkun, S., 2011. Acoustic evidence of
1700
1701 631 shallow gas accumulations and active pockmarks in the İzmir Gulf, Aegean sea.
1702
1703 632 *Mar. Pet. Geol.* 28, 1505–1516.
- 1704
1705 633 Dowling, N.J.E., Widdel, F., White, D.C., 1986. Phospholipid Ester-linked Fatty
1706
1707 634 Acid Biomarkers of Acetate-oxidizing Sulphate-reducers and Other Sulphide-
1708
1709 635 forming Bacteria. *Microbiology* 132, 1815–1825.
- 1710
1711 636 Elvert, M., Boetius, A., Knittel, K., Jørgensen, B.B., 2003. Characterization of
1712
1713 637 Specific Membrane Fatty Acids as Chemotaxonomic Markers for Sulfate-
1714
1715 638 Reducing Bacteria Involved in Anaerobic Oxidation of Methane. *Geomicrobiol.*
1716
1717 639 *J.* 20, 403–419.
- 1718
1719 640 Etiope, G., Milkov, A., Derbyshire, E., 2008. Did geologic emissions of methane
1720
1721 641 play any role in Quaternary climate change? *Glob. Planet. Change* 61, 79–88.
- 1722
1723 642 Faber, E., Stahl, W., 1984. Geochemical surface exploration for hydrocarbons in
1724
1725 643 North Sea. *Am. Assoc. Pet. Geol. Bull.* 68, 363–386.
- 1726
1727 644 Field, M.E., Jennings, A.E., 1987. Seafloor gas seeps triggered by a northern
1728
1729 645 California earthquake. *Mar. Geol.* 77, 39–51.
- 1730
1731 646 Findlay, R.H., Trexler, M.B., Guckert, J.B., White, D.C., 1990. Laboratory study of
1732
1733 647 disturbance in marine sediments: response of a microbial community. *Mar.*
1734
1735 648 *Ecol. Prog. Ser. Oldend.* 62, 121–133.
- 1736
1737
1738
1739
1740
1741
1742
1743

- 1744
1745
1746 649 Floodgate, G.D., Judd, a. G., 1992. The origins of shallow gas. *Cont. Shelf Res.* 12,
1747
1748 650 1145–1156.
1749
1750
1751 651 Froelich, P.N., Klinkhammer, G.P., Bender, M.L., Luedtke, N.A., Heath, G.R.,
1752
1753 652 Cullen, D., Dauphin, P., Hammond, D., Hartman, B., Maynard, V., 1979. Early
1754
1755 653 oxidation of organic matter in pelagic sediments of the eastern equatorial
1756
1757 654 Atlantic: suboxic diagenesis. *Geochim. Cosmochim. Acta* 43, 1075–1090.
1758
1759 655 Gauthier, M., Bradley, R.L., Šimek, M., 2015. More evidence that anaerobic
1760
1761 656 oxidation of methane is prevalent in soils: Is it time to upgrade our
1762
1763 657 biogeochemical models? *Soil Biol. Biochem.* 80, 167–174.
1764
1765 658 Gay, a., Lopez, M., Berndt, C., Séranne, M., 2007. Geological controls on focused
1766
1767 659 fluid flow associated with seafloor seeps in the Lower Congo Basin. *Mar. Geol.*
1768
1769 660 244, 68–92.
1770
1771 661 Ge, L., Jiang, S.-Y., Blumenberg, M., Reitner, J., 2015. Lipid biomarkers and their
1772
1773 662 specific carbon isotopic compositions of cold seep carbonates from the South
1774
1775 663 China Sea. *Mar. Pet. Geol.* 66, 501–510.
1776
1777 664 Hammer, Ø., Webb, K.E., Depreiter, D., 2009. Numerical simulation of upwelling
1778
1779 665 currents in pockmarks, and data from the Inner Oslofjord, Norway. *Geo-Marine*
1780
1781 666 *Lett.* 29, 269–275.
1782
1783 667 Hasiotis, T., Papatheodorou, G., Kastanos, N., Ferentinos, G., 1996. A pockmark
1784
1785 668 field in the Patras Gulf (Greece) and its activation during the 14/7/93 seismic
1786
1787 669 event. *Mar. Geol.* 130, 333–344.
1788
1789
1790 670 Hovland, M., 1989. The formation of pockmarks and their potential influence on
1791
1792 671 offshore construction. *Q. J. Eng. Geol. Hydrogeol.* 22, 131–138.
1793
1794 672 Hovland, M., 2013. Characteristics of Marine Methane Macroseeps. In: Aminzadeh,
1795
1796 673 F., Berge, T.B., Connolly, D.L. (Eds.), *Hydrocarbon Seepage: From Source to*

- 1804
1805
1806 674 Surface. Society of Exploration Geophysicists (SEG), and American
1807
1808 675 Association of Petroleum Geologists (AAPG), pp. 63–82.
1809
1810 676 Hovland, M., Gardner, J. V., Judd, a. G., 2002. The significance of pockmarks to
1811
1812 677 understanding fluid flow processes and geohazards. *Geofluids* 2, 127–136.
1813
1814 678 Hovland, M., Judd, A.G., 1988. Seabed pockmarks and seepages: impact on
1815
1816 679 geology, biology, and the marine environment. Graham and Trotman, London.
1817
1818 680 Janssen, F., Huettel, M., Witte, U., 2005. Pore-water advection and solute fluxes in
1819
1820 681 permeable marine sediments (II): Benthic respiration at three sandy sites with
1821
1822 682 different permeabilities (German Bight, North Sea). *Limnol. Oceanogr.* 50,
1823
1824 683 779–792.
1825
1826 684 Joye, S.B., Connell, T.L., Miller, L.G., Oremland, R.S., Jellison, R.S., 1999.
1827
1828 685 Oxidation of ammonia and methane in an alkaline, saline lake. *Limnol.*
1829
1830 686 *Oceanogr.* 44, 178–188.
1831
1832 687 Judd, A., Hovland, M., 2009. Seabed Fluid Flow - The Impact on Geology, Biology
1833
1834 688 and the Marine Environment. Cambridge University Press, Cambridge.
1835
1836 689 King, L.H., MacLean, B., 1970. Pockmarks on the Scotian Shelf. *Geol. Soc. Am.*
1837
1838 690 *Bull.* 81, 3141–3148.
1839
1840 691 King, L.L., Pease, T.K., Wakeham, S.G., 1998. Archaea in Black Sea water column
1841
1842 692 particulate matter and sediments—evidence from ether lipid derivatives. *Org.*
1843
1844 693 *Geochem.* 28, 677–688.
1845
1846 694 Knittel, K., Boetius, A., 2009. Anaerobic Oxidation of Methane: Progress with an
1847
1848 695 Unknown Process. *Annu. Rev. Microbiol.* 63, 311–334.
1849
1850 696 Li, Y., Peacock, a, White, D., Geyer, R., Zhang, C., 2007. Spatial patterns of
1851
1852 697 bacterial signature biomarkers in marine sediments of the Gulf of Mexico.
1853
1854 698 *Chem. Geol.* 238, 168–179.
1855
1856
1857
1858
1859
1860
1861
1862
1863

- 1864
1865
1866 699 Lin, Q., Wang, J., Algeo, T.J., Sun, F., Lin, R., 2016. Enhanced framboidal pyrite
1867
1868 700 formation related to anaerobic oxidation of methane in the sulfate-methane
1869
1870 701 transition zone of the northern South China Sea. *Mar. Geol.* 379, 100–108.
1871
1872
1873 702 Locat, J., Lee, H.J., 2002. Submarine landslides: advances and challenges. *Can.*
1874
1875 703 *Geotech. J.* 39, 193–212.
1876
1877 704 Navarrete, A., Peacock, A., Macnaughton, S., Urmeneta, J., Mas-Castellà, J., White,
1878
1879 705 D., Guerrero, R., 2000. Physiological Status and Community Composition of
1880
1881 706 Microbial Mats of the Ebro Delta, Spain, by Signature Lipid Biomarkers.
1882
1883 707 *Microb. Ecol.* 39, 92–99.
1884
1885 708 Nichols, P.D., Guckert, J.B., White, D.C., 1986. Determination of monosaturated
1886
1887 709 fatty acid double-bond position and geometry for microbial monocultures and
1888
1889 710 complex consortia by capillary GC-MS of their dimethyl disulphide adducts. *J.*
1890
1891 711 *Microbiol. Methods* 5, 49–55.
1892
1893 712 Niemann, H., Elvert, M., 2008. Diagnostic lipid biomarker and stable carbon isotope
1894
1895 713 signatures of microbial communities mediating the anaerobic oxidation of
1896
1897 714 methane with sulphate. *Org. Geochem.* 39, 1668–1677.
1898
1899 715 O'Reilly, S.S., Hryniewicz, K., Little, C.T.S., Monteys, X., Szpak, M.T., Murphy,
1900
1901 716 B.T., Jordan, S.F., Allen, C.C.R., Kelleher, B.P., 2014. Shallow water methane-
1902
1903 717 derived authigenic carbonate mounds at the Codling Fault Zone, western Irish
1904
1905 718 Sea. *Mar. Geol.* 357, 139–150.
1906
1907 719 Pancost, R.D., Sinninghe Damste, J.S., de Lint, S., van der Maarel, M.J.E.C.,
1908
1909 720 Gottschal, J.C., 2000. Biomarker Evidence for Widespread Anaerobic Methane
1910
1911 721 Oxidation in Mediterranean Sediments by a Consortium of Methanogenic
1912
1913 722 Archaea and Bacteria. *Appl. Environ. Microbiol.* 66, 1126–1132.
1914
1915
1916
1917 723 Pau, M., Gisler, G., Hammer, Ø., 2014. Experimental investigation of the
1918
1919
1920
1921
1922
1923

- 1924
1925
1926 724 hydrodynamics in pockmarks using particle tracking velocimetry. *Geo-Marine*
1927
1928 725 *Lett.* 34, 11–19.
1929
1930 726 Pinkart, H.C., Devereux, R., Chapman, P.J., 1998. Rapid separation of microbial
1931
1932 727 lipids using solid phase extraction columns. *J. Microbiol. Methods* 34, 9–15.
1933
1934 728 Plets, R.M.K., Callard, S.L., Cooper, J.A.G., Long, A.J., Quinn, R.J., Belknap, D.F.,
1935
1936 729 Edwards, R.J., Jackson, D.W.T., Kelley, J.T., Long, D., Milne, G.A., Monteys,
1937
1938 730 X., 2015. Late Quaternary evolution and sea-level history of a glaciated marine
1939
1940 731 embayment, Bantry Bay, SW Ireland. *Mar. Geol.* 369, 251–272.
1941
1942 732 Rajendran, N., Matsuda, O., Imamura, N., Urushigawa, Y., 1992. Variation in
1943
1944 733 Microbial Biomass and Community Structure in Sediments of Eutrophic Bays
1945
1946 734 as Determined by Phospholipid Ester-Linked Fatty Acids. *Appl. Envir.*
1947
1948 735 *Microbiol.* 58, 562–571.
1949
1950 736 Rajendran, N., Matsuda, O., Imamura, N., Urushigawa, Y., 1995. Microbial
1951
1952 737 community structure analysis of euxinic sediments using phospholipid fatty
1953
1954 738 acid biomarkers. *J. Oceanogr.* 51, 21–38.
1955
1956 739 Reeburgh, W.S., 2007. Oceanic Methane Biogeochemistry. *Chem. Rev.* 107, 486–
1957
1958 740 513.
1959
1960 741 Ringelberg, D.B., Sutton, S., White, D.C., 1997. Biomass, bioactivity and
1961
1962 742 biodiversity: microbial ecology of the deep subsurface: analysis of ester-linked
1963
1964 743 phospholipid fatty acids. *FEMS Microbiol. Rev.* 20, 371–377.
1965
1966 744 Römer, M., Torres, M., Kasten, S., Kuhn, G., Graham, A.G.C., Mau, S., Little,
1967
1968 745 C.T.S., Linse, K., Pape, T., Geprägs, P., Fischer, D., Wintersteller, P., Marcon,
1969
1970 746 Y., Rethemeyer, J., Bohrmann, G., 2014. First evidence of widespread active
1971
1972 747 methane seepage in the Southern Ocean, off the sub-Antarctic island of South
1973
1974 748 Georgia. *Earth Planet. Sci. Lett.* 403, 166–177.
1975
1976
1977
1978
1979
1980
1981
1982
1983

1984
1985
1986
1987
1988
1989
1990
1991
1992
1993
1994
1995
1996
1997
1998
1999
2000
2001
2002
2003
2004
2005
2006
2007
2008
2009
2010
2011
2012
2013
2014
2015
2016
2017
2018
2019
2020
2021
2022
2023
2024
2025
2026
2027
2028
2029
2030
2031
2032
2033
2034
2035
2036
2037
2038
2039
2040
2041
2042
2043

749 Ruff, S.E., Kuhfuss, H., Wegener, G., Lott, C., Ramette, A., Wiedling, J., Knittel,
750 K., Weber, M., 2016. Methane Seep in Shallow-Water Permeable Sediment
751 Harbors High Diversity of Anaerobic Methanotrophic Communities, Elba, Italy
752 . *Front. Microbiol.* .
753 Schouten, S., Hopmans, E.C., Sinninghe Damsté, J.S., 2013. The organic
754 geochemistry of glycerol dialkyl glycerol tetraether lipids: A review. *Org.*
755 *Geochem.* 54, 19–61.
756 Shakhova, N., Semiletov, I., Salyuk, A., Yusupov, V., Kosmach, D., Gustafsson, O.,
757 2010. Extensive methane venting to the atmosphere from sediments of the East
758 Siberian Arctic Shelf. *Science* 327, 1246–50.
759 Skarke, A., Ruppel, C., Kodis, M., Brothers, D., Lobecker, E., 2014. Widespread
760 methane leakage from the sea floor on the northern US Atlantic margin. *Nat.*
761 *Geosci* 7, 657–661.
762 Soter, S., 1999. Macroscopic seismic anomalies and submarine pockmarks in the
763 Corinth–Patras rift, Greece. *Tectonophysics* 308, 275–290.
764 Stillman, C.J., 1968. The Post Glacial Change in Sea Level in Southwestern Ireland:
765 New Evidence from Fresh-water Deposits on the Floor of Bantry Bay, The
766 scientific proceedings of the Royal Dublin Society. Royal Dublin Society.
767 Szpak, M.T., Monteys, X., O’Reilly, S., Simpson, A.J., Garcia, X., Evans, R.L.,
768 Allen, C.C.R., McNally, D.J., Courtier-Murias, D., Kelleher, B.P., 2012.
769 Geophysical and geochemical survey of a large marine pockmark on the Malin
770 Shelf, Ireland. *Geochemistry, Geophys. Geosystems* 13.
771 Szpak, M.T., Monteys, X., O’Reilly, S.S., Lilley, M.K.S., Scott, G.A., Hart, K.M.,
772 McCarron, S.G., Kelleher, B.P., 2015. Occurrence, characteristics and
773 formation mechanisms of methane generated micro-pockmarks in Dunmanus

- 2044
2045
2046 774 Bay, Ireland. *Cont. Shelf Res.* 103, 45–59.
2047
- 2048 775 Taylor, J., Parkes, R.J., 1983. The Cellular Fatty Acids of the Sulphate-reducing
2049
2050 776 Bacteria, *Desulfobacter* sp., *Desulfobulbus* sp. and *Desulfovibrio desulfuricans*.
2051
2052 777 *Microbiology* 129, 3303–3309.
2053
2054
- 2055 778 Trent, J.D., Kagawa, H.K., Paavola, C.D., McMillan, R.A., Howard, J., Jahnke, L.,
2056
2057 779 Lavin, C., Embaye, T., Henze, C.E., 2003. Intracellular localization of a group
2058
2059 780 II chaperonin indicates a membrane-related function. *Proc. Natl. Acad. Sci. U.*
2060
2061 781 *S. A.* 100, 15589–15594.
2062
- 2063 782 Valentine, D.L., 2002. Biogeochemistry and microbial ecology of methane oxidation
2064
2065 783 in anoxic environments: a review. *Antonie Van Leeuwenhoek* 81, 271–282.
2066
2067
- 2068 784 Valentine, D.L., Reeburgh, W.S., 2000. New perspectives on anaerobic methane
2069
2070 785 oxidation. *Environ. Microbiol.* 2, 477–484.
2071
- 2072 786 van Dongen, B.E., Roberts, A.P., Schouten, S., Jiang, W.-T., Florindo, F., Pancost,
2073
2074 787 R.D., 2007. Formation of iron sulfide nodules during anaerobic oxidation of
2075
2076 788 methane. *Geochim. Cosmochim. Acta* 71, 5155–5167.
2077
- 2078 789 Verardo, D.J., Froelich, P.N., McIntyre, A., 1990. Determination of organic carbon
2079
2080 790 and nitrogen in marine sediments using the Carlo Erba NA-1500 analyzer. *Deep*
2081
2082 791 *Sea Res. Part A. Oceanogr. Res. Pap.* 37, 157–165.
2083
2084
- 2085 792 Vermeulen, N.J., Shannon, P.M., Masson, F., Landes, M., 2000. Wide-angle seismic
2086
2087 793 control on the development of the Munster Basin, SW Ireland. *Geol. Soc.*
2088
2089 794 *London, Spec. Publ.* 180, 223–237.
2090
- 2091 795 Volkman, J.K., Johns, R.B., Gillan, F.T., Perry, G.J., Bavor, H.J., 1980. Microbial
2092
2093 796 lipids of an intertidal sediment—I. Fatty acids and hydrocarbons. *Geochim.*
2094
2095 797 *Cosmochim. Acta* 44, 1133–1143.
2096
2097
- 2098 798 Wakeham, S.G., Lewis, C.M., Hopmans, E.C., Schouten, S., Sinninghe Damsté, J.S.,
2099
2100
2101
2102
2103

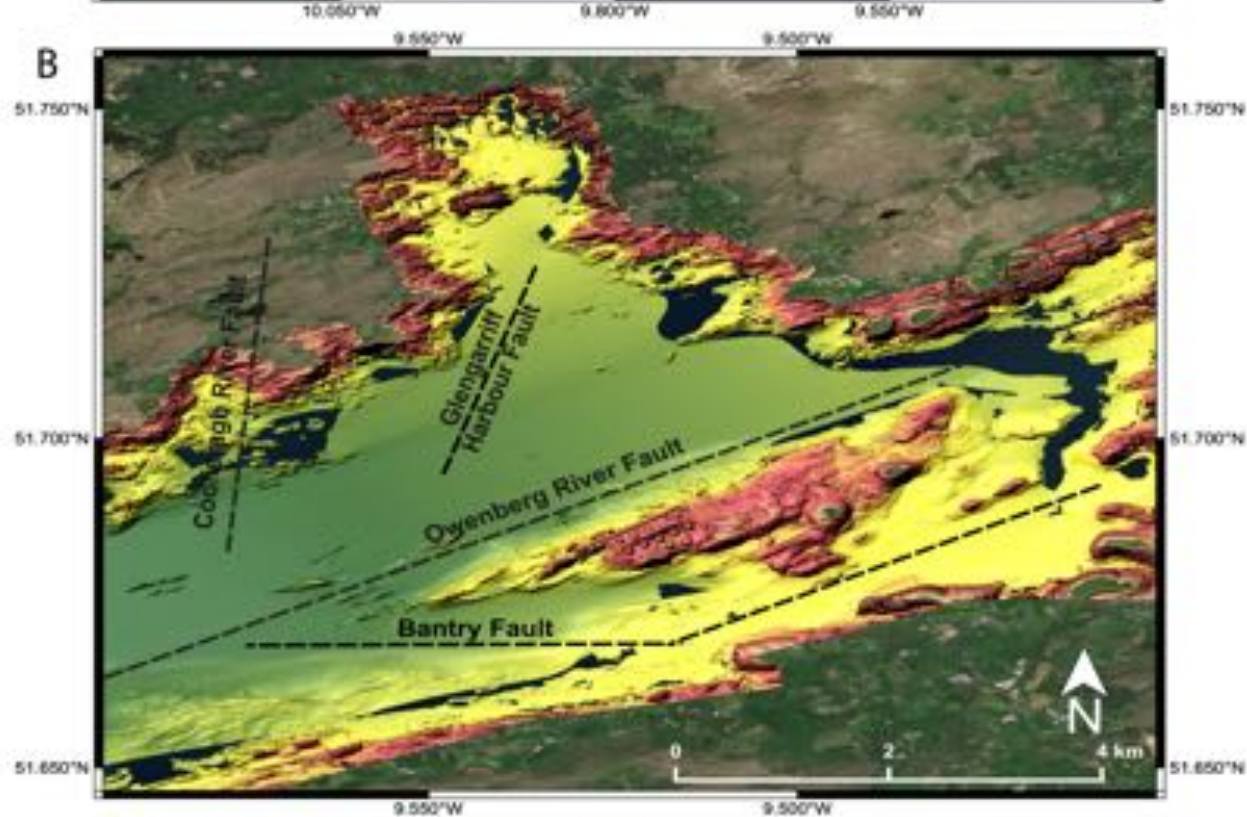
- 2104
2105
2106 799 2003. Archaea mediate anaerobic oxidation of methane in deep euxinic waters
2107
2108 800 of the Black Sea. *Geochim. Cosmochim. Acta* 67, 1359–1374.
2109
2110 801 Westbrook, G.K., Thatcher, K.E., Rohling, E.J., Piotrowski, A.M., Pälike, H.,
2111
2112 802 Osborne, A.H., Nisbet, E.G., Minshull, T.A., Lanoisellé, M., James, R.H.,
2113
2114 803 Hühnerbach, V., Green, D., Fisher, R.E., Crocker, A.J., Chabert, A., Bolton, C.,
2115
2116 804 Beszczynska-Möller, A., Berndt, C., Aquilina, A., 2009. Escape of methane gas
2117
2118 805 from the seabed along the West Spitsbergen continental margin. *Geophys. Res.*
2119
2120 806 *Lett.* 36.
2121
2122
2123 807 Wheeler, A.J., 2002. Environmental controls on shipwreck preservation: The Irish
2124
2125 808 context. *J. Archaeol. Sci.* 29, 1149–1159.
2126
2127 809 White, D.C., Ringelberg, D.B., MacNaughton, S.J., Srinivas, A., Schram, D., 1997.
2128
2129 810 Signature Lipid Biomarker Analysis for Quantitative Assessment In Situ of
2130
2131 811 Environmental Microbial Ecology. In: Eganhouse, R.P. (Ed.), *Molecular*
2132
2133 812 *Markers in Environmental Chemistry*. American Chemical Society, Washington
2134
2135 813 D.C., pp. 22–34.
2136
2137 814 Yvon-Durocher, G., Allen, A.P., Bastviken, D., Conrad, R., Gudas, C., St-Pierre,
2138
2139 815 A., Thanh-Duc, N., del Giorgio, P.A., 2014. Methane fluxes show consistent
2140
2141 816 temperature dependence across microbial to ecosystem scales. *Nature* 507, 488–
2142
2143 817 491.
2144
2145 818 Zelles, L., 1997. Phospholipid fatty acid profiles in selected members of soil
2146
2147 819 microbial communities. *Chemosphere* 35, 275–294.
2148
2149
2150
2151 820
2152
2153
2154
2155
2156
2157
2158
2159
2160
2161
2162
2163

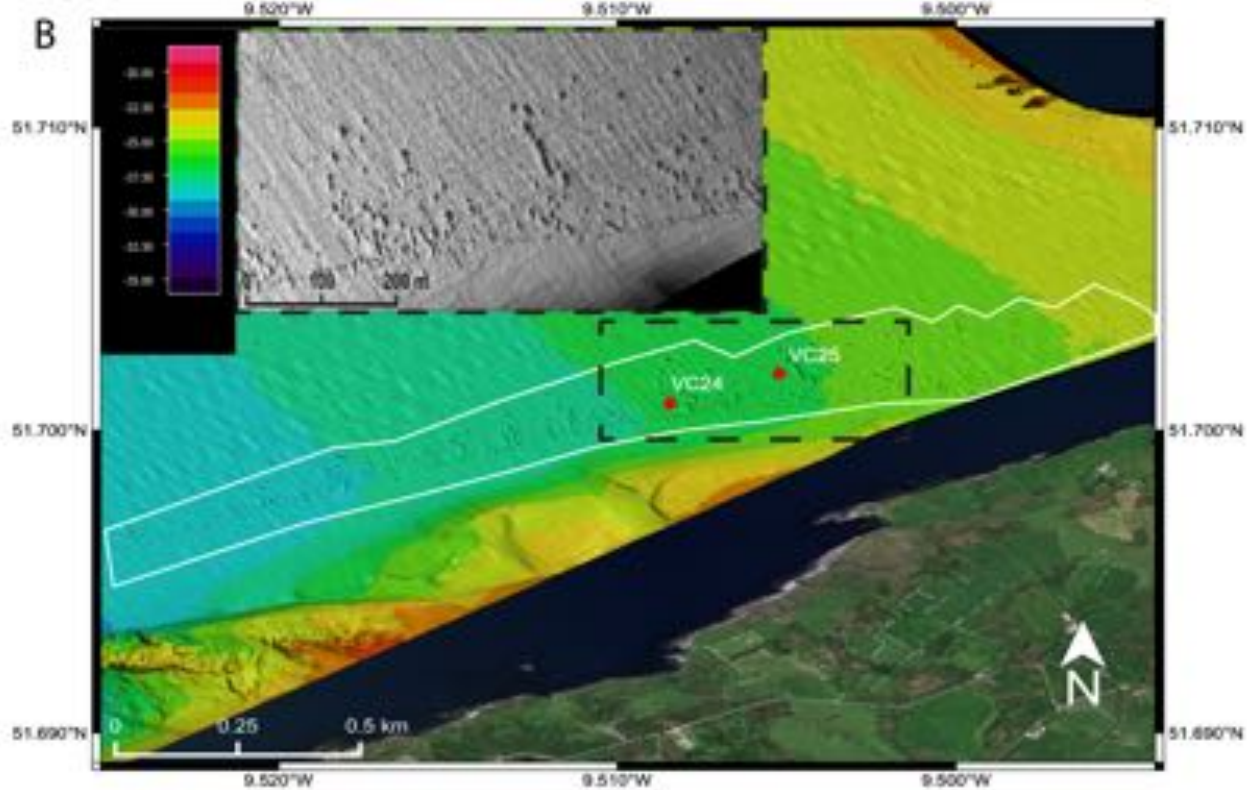
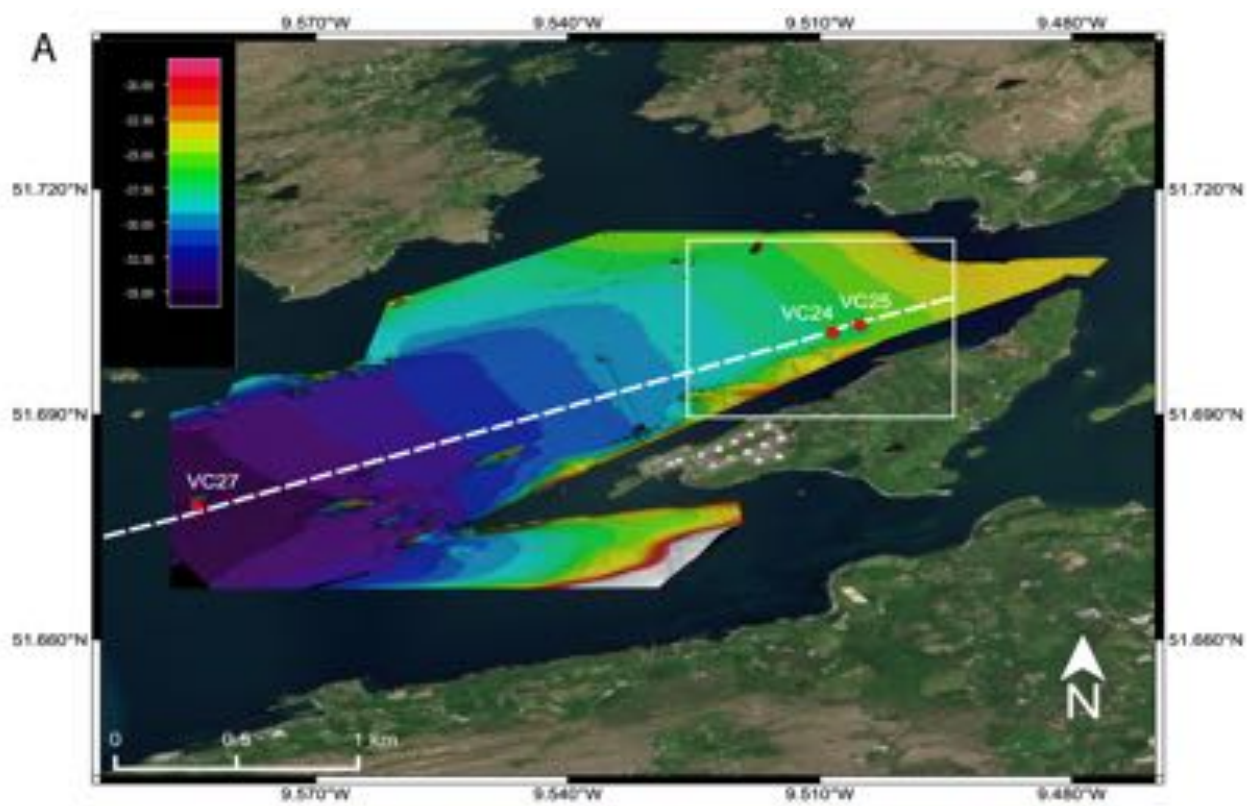
Figure 1. (A) Map of Bantry Bay and surrounding area, location of Bantry Bay within Ireland (inset). (B) Bathymetric map of inner Bantry Bay showing locations of underlying faults.

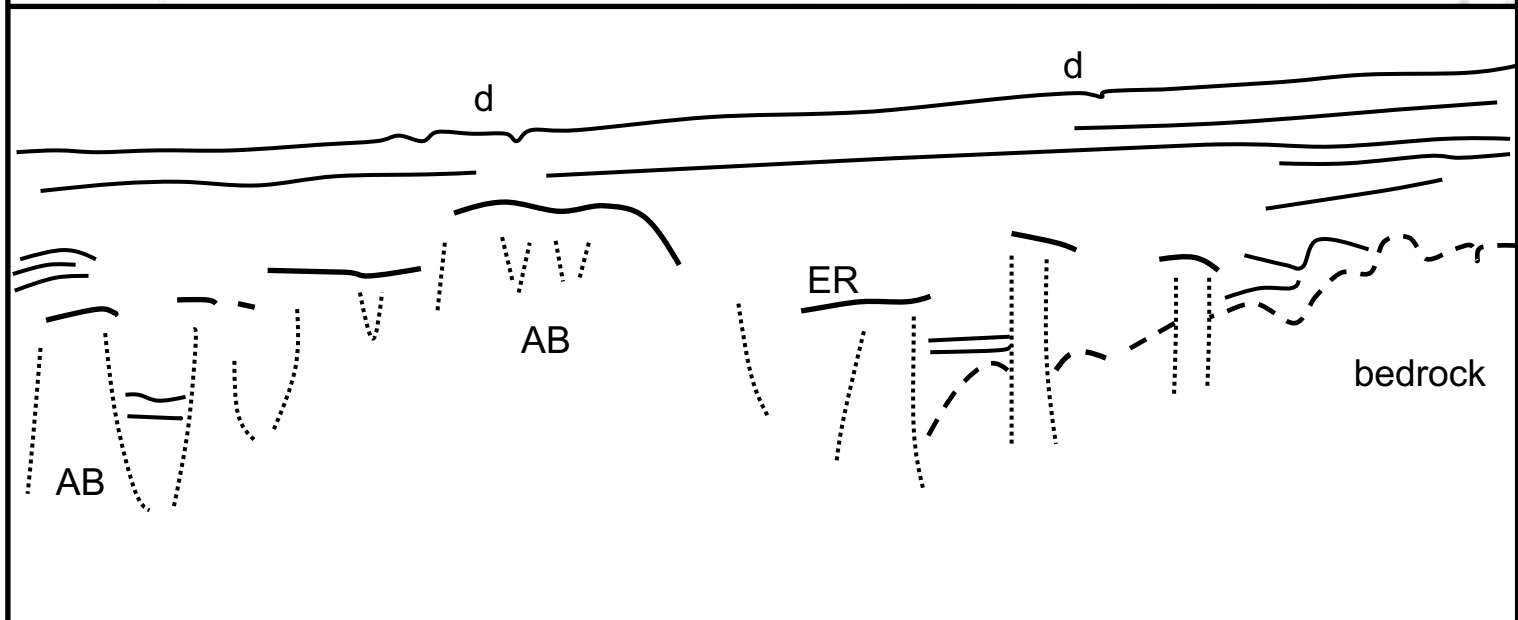
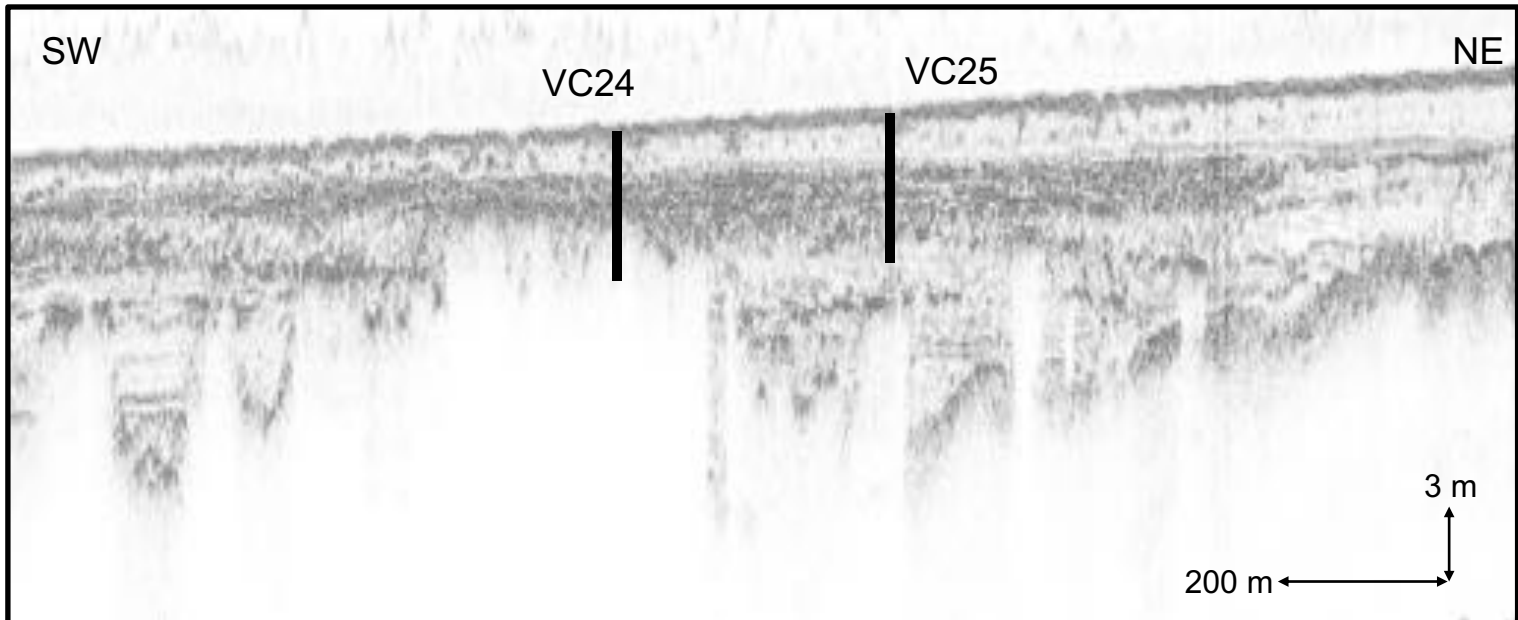
Figure 2. (A) Bathymetric map of inner Bantry Bay, vibrocore locations marked with red dots. The pockmark field north of Whiddy Island is located within the white box. (B) Close up of pockmark field from (A) with the entire field highlighted by a white outline and vibrocore locations marked with red dots. A close up of the section of the pockmark field within the black dashed rectangle is also depicted (inset).

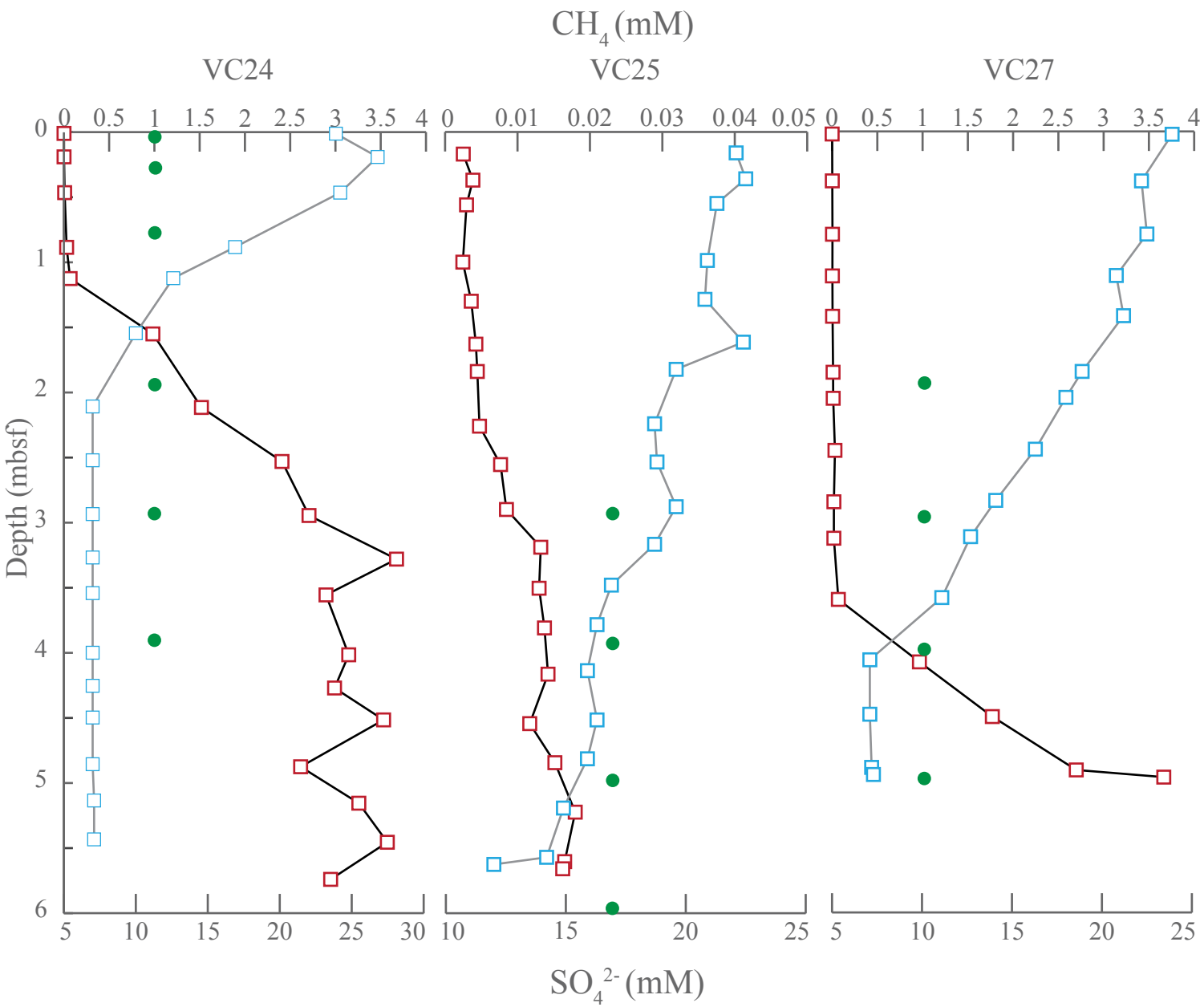
Figure 3. Sub-bottom profiles taken at the site of VC24 and VC25 vibrocores showing sampling locations (black line), enhanced reflectors (ER), and acoustic blanking (AB).

Figure 4. CH₄ (mM) and SO₄²⁻ (mM) profiles for each core. Green dots represent sub-sampling locations for lipid biomarker analysis.









- CH_4
- SO_4^{2-}
- Biomarker Sample

Supporting Information

Geophysical and geochemical analysis of shallow gas and an associated pockmark field in Bantry Bay, Co. Cork, Ireland.

S.F. Jordan^a, S.S. O'Reilly^b, D. Praeg^{c,d}, D. Dove^e, L. Facchin^d, R. Romeo^d, M. Szpak^f, X. Monteys^f, B.T. Murphy^a, G. Scott^g, S.S. McCarron^g, and B.P. Kelleher^{a,*}

^a *School of Chemical Sciences, Dublin City University, Dublin 9, Ireland*

^b *Department of Earth, Atmospheric, and Planetary Sciences, Massachusetts Institute of Technology, Cambridge, MA, USA*

^c *Géoazur (UMR7329 CNRS), 250 Rue Albert Einstein, 06560 Valbonne, France*

^d *OGS (Istituto Nazionale di Oceanografia e di Geofisica Sperimentale), Borgo Grotta Gigante 42C, Trieste, 34010, Italy*

^e *British Geological Survey, The Lyell Centre, Research Avenue South, Edinburgh, EH14 4AP, UK*

^f *Geological Survey of Ireland, Beggars Bush, Haddington Road, Dublin, Ireland*

^g *Maynooth University Department of Geography, Maynooth, Co. Kildare, Ireland*

*Corresponding author: *E-mail address:* brian.kelleher@dcu.ie (B.P. Kelleher).

Results

Table S1. CH₄ (μM) and SO₄²⁻ (mM) data from geochemical analysis of vibrocores.

VC24			VC25			VC27		
Depth (mbsf)	CH ₄ (μM)	SO ₄ ²⁻ (mM)	Depth (mbsf)	CH ₄ (μM)	SO ₄ ²⁻ (mM)	Depth (mbsf)	CH ₄ (μM)	SO ₄ ²⁻ (mM)
0.01	1.5	23.9	0.17	2.5	22.1	0.02	0.9	23.9
0.19	1.8	26.8	0.37	3.8	22.5	0.38	2.6	22.2
0.47	8.6	24.2	0.56	3.0	21.3	0.79	4.5	22.5
0.89	30.5	16.9	1.00	2.5	20.9	1.11	3.8	20.8
1.13	68.9	12.6	1.30	3.6	20.8	1.42	5.5	21.2
1.55	983.5	10.0	1.63	4.2	22.4	1.85	11.2	18.9
2.12	1519.6	7.0	1.84	4.4	19.6	2.05	12.4	18.0
2.53	2409.5	7.0	2.26	4.8	18.7	2.45	31.9	16.3
2.95	2707.7	7.0	2.56	7.7	18.8	2.85	20.3	14.1
3.28	3674.9	7.0	2.90	8.5	19.6	3.13	19.9	12.7
3.56	2895.5	7.0	3.19	13.2	18.7	3.60	69.6	11.1
4.02	3146.6	7.0	3.51	13.0	16.9	4.08	964.9	7.1
4.27	2989.9	7.0	3.81	13.7	16.3	4.50	1770.4	7.1
4.52	3531.9	7.0	4.17	14.2	15.9	4.91	2697.4	7.2
4.88	2615.2	7.0	4.55	11.7	16.3	4.96	3664.2	7.3
5.16	3258.2	7.1	4.85	15.2	15.9			
5.46	3573.0	7.1	5.23	18.0	14.9			
5.74	2946.9		5.61	16.5	14.2			
			5.66	16.2	12.0			

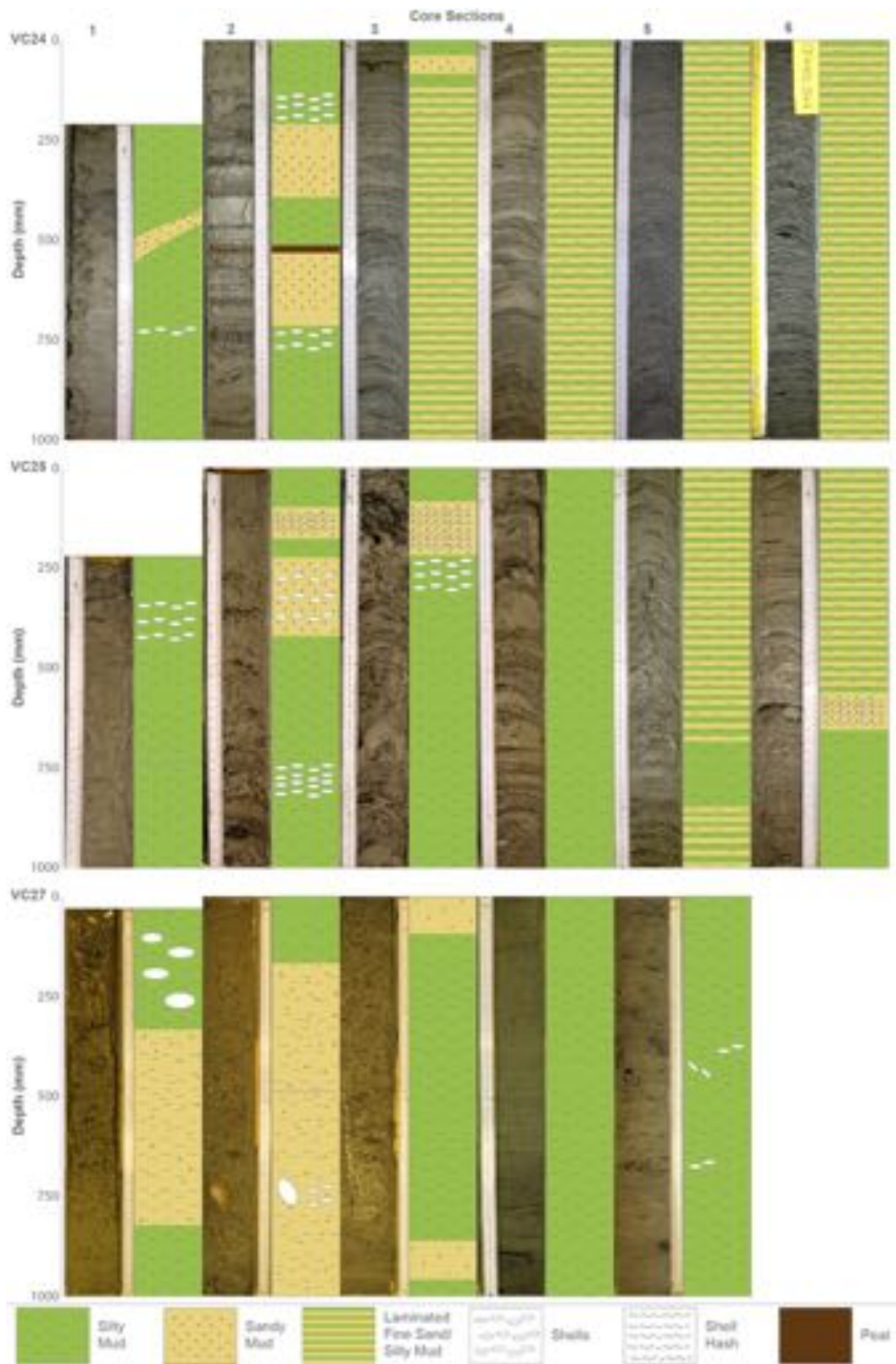


Fig. S1. Photographs of vibrocore sections taken onboard the *RV Celtic Explorer* during research cruise CE14003. Graphical depictions of sediment type from core logs are displayed alongside relevant sections.